

A study of the global cycle of carbonaceous aerosols in the LMDZT general circulation model

M. Shekar Reddy and Olivier Boucher

Laboratoire d'Optique Atmosphérique/CNRS, Université des Sciences et Technologies de Lille, Villeneuve d'Ascq, France

Received 5 August 2003; revised 13 February 2004; accepted 28 April 2004; published 20 July 2004.

[1] The global atmospheric cycle of carbonaceous aerosols is simulated in the Laboratoire de Météorologie Dynamique general circulation model, and the subsequent aerosol optical depth is estimated for the period 1997 to 1999. The seasonal and interannual variability in the open biomass burning emissions has been improved by combining existing emission inventories and satellite measured fire counts. The model performance has been thoroughly evaluated against measured aerosol mass concentrations and optical depth in different regions of the globe. At a majority of locations, the modeled mass concentrations of black carbon (BC) at the surface are within a factor of two of observed values. The concentrations of organic carbon (OC) are generally underestimated in comparison to measurements. The discrepancies between model predicted values and measurements are attributable to the difference in time periods between the measurements and model simulations and/or a real underestimation of aerosol emissions in the model. The atmospheric residence times of both BC and OC aerosols are about a week. The hydrophilic fraction of carbonaceous aerosols accounts for about 90% of the total burden. Organic matter (OM) and associated water dominate the optical depth by carbonaceous aerosols with a 86% contribution (global mean of 0.031 at 0.55 μm). Different sensitivity experiments on the transformation time for conversion of hydrophobic to hydrophilic aerosols and emission partitioning show significant changes in the distribution of aerosol burdens and optical depth. The globally averaged burdens change by $\pm 15\%$ and residence times are shorter or longer by about 1 day in the various experiments as compared to the control simulation. In all of these experiments the largest sensitivity in aerosol concentrations is found in the remote regions and in the free troposphere (pressure range of 700–400 hPa). Emissions from biomass burning dominate the burden and optical depth of carbonaceous aerosols in the entire SH and NH tropics, while fossil fuel emissions dominate the NH extratropics. On the global scale biomass burning accounts for 78% of the total carbonaceous aerosol burden (BC + OM) followed by natural secondary organic aerosols (SOA)(14%) and fossil fuels (8%). The contributions to corresponding AOD are similar with the largest contribution from biomass burning (76%) followed by natural SOA (14%), and fossil fuels (10%).

INDEX TERMS: 0305 Atmospheric Composition and Structure: Aerosols and particles (0345, 4801); 0345 Atmospheric Composition and Structure: Pollution—urban and regional (0305); 0365 Atmospheric Composition and Structure: Troposphere—composition and chemistry; *KEYWORDS:* carbonaceous aerosols, model validation, sensitivity studies

Citation: Reddy, M. S., and O. Boucher (2004), A study of the global cycle of carbonaceous aerosols in the LMDZT general circulation model, *J. Geophys. Res.*, 109, D14202, doi:10.1029/2003JD004048.

1. Introduction

[2] Radiative forcing by aerosols is recognized as an important contributor to climate change. The change in the reflected radiation at the top of the atmosphere due to scattering sulfate aerosols ranges from -0.3 Wm^{-2} to -0.9 Wm^{-2} [Kiehl and Briegleb, 1993; Boucher and Anderson, 1995; Adams *et al.*, 2001]. Carbonaceous aerosols, mainly produced from fossil fuel and biomass com-

bustion, are now considered as being as important as sulfate aerosols. They are composed of two components, black carbon (BC) and organic carbon (OC). Black carbon is only emitted directly from primary sources whereas OC is either emitted by direct sources (primary OC) or condensed in the atmosphere from volatile organic compounds (secondary OC). Oxygen, hydrogen, and other chemical species are always associated with OC, and the resulting aerosol is called organic matter (OM). While OM is mainly scattering BC strongly absorbs solar radiation with an estimated mass absorption coefficient of $7\text{--}12 \text{ m}^2\text{g}^{-1}$ at 0.55 μm [Horvath *et al.*, 1986; Japar *et al.*, 1986]. Absorption by BC lowers

the aerosol single scattering albedo, thereby increasing the amount of radiation absorbed in the atmosphere [Haywood and Shine, 1995], leading to a net heating of the atmosphere. The direct radiative forcing by OC is generally considered to be negative while the forcing by BC is positive. Ramaswamy *et al.* [2001] give radiative forcing estimates of $+0.2 \text{ Wm}^{-2}$ and a factor of two uncertainty for fossil-fuel BC and -0.1 Wm^{-2} and a factor of three uncertainty for fossil-fuel OC. The radiative effects of biomass burning aerosols were not separated between their OC and BC contributions and an estimate of -0.2 Wm^{-2} has been given with a factor of three uncertainty.

[3] The global distribution of carbonaceous aerosols have been estimated in a number of studies [Cooke and Wilson, 1996; Lioussse *et al.*, 1996; Penner *et al.*, 1998; Cooke *et al.*, 1999, 2002; Takemura *et al.*, 2000; Koch, 2001; Chung and Seinfeld, 2002; Chuang *et al.*, 2002; Chin *et al.*, 2002]. It has been shown in particular that their atmospheric burden and residence time are functions of the assumed state of emissions (hydrophobic and/or hydrophilic) and aerosol hygroscopicity [Cooke *et al.*, 2002].

[4] In this work we simulate the atmospheric cycle of carbonaceous aerosols and estimate aerosol optical depth (AOD) in the LMDZT GCM (Laboratoire de Météorologie Dynamique, general circulation model). This modeling work follows from a previous study of the global sulfate aerosol cycling and radiative forcing in the LMDZT GCM [Boucher *et al.*, 2002; Boucher and Pham, 2002]. The open biomass burning emissions are known to be region specific and highly seasonal dependent. Here, we combine existing aerosol emission inventories and satellite-derived fire counts to improve the seasonality of these emissions. The performance of the model is validated through comparison with available measurements of mass concentrations in different parts of the globe. In Africa and South America the model AOD is also compared with measured AOD from sunphotometers. We also present the sensitivity of the aerosol burdens and residence times to the assumed state of the emissions and transformation time (λ) from hydrophobic to hydrophilic BC and OM. These sensitivity experiments are similar to those conducted by Cooke *et al.* [2002] but include both fossil-fuel and biomass burning sources of BC and OM. An estimate of the contribution of various emission sources to the burden and optical depth of carbonaceous aerosols is also presented.

2. Model Description

2.1. General Description

[5] The three-dimensional global cycle of carbonaceous aerosols is simulated in the LMD-ZT version 3.3. Atmospheric transport is computed with a finite volume transport scheme for large-scale advection [van Leer, 1977; Hourdin and Armangaud, 1999], a scheme for turbulent mixing in the boundary layer, and a mass flux scheme for convection [Tiedtke, 1989]. The model resolution is 3.75° in longitude and 2.5° in latitude (corresponding roughly to the resolution of a T46 spectral model (F. Hourdin, personal communication)). In the present version there are 19 vertical layers, with a hybrid sigma-pressure coordinate, with 5 layers below about 600 hPa and 9 layers above about 250 hPa. The time step is 3 min for resolving the dynamical part of

the primitive equations. Mass fluxes are cumulated over five time steps so that large-scale advection is applied every 15 min. The physical and chemical parameterizations are applied every 10 time steps or 30 min. The different processes are handled through operator splitting. In the present version of the model we consider four different classes of carbonaceous aerosols, namely hydrophobic BC, hydrophilic BC, hydrophobic OM, and hydrophilic OM.

2.2. Aerosol Emissions

[6] Major sources of carbonaceous aerosol emissions are from fossil fuel and biomass combustion. Existing global carbonaceous inventories include those of Penner *et al.* [1993], Lioussse *et al.* [1996], Cooke and Wilson [1996], hereafter referred as CW96, Cooke *et al.* [1999], and Bond *et al.* [2004]. Recently regional emission inventories for Asia [Streets *et al.*, 2003] and India [Reddy and Venkataraman, 2002a, 2002b] were also developed. Differences among these inventories arise mainly from the amount of biomass burnt and the emission factors used for fossil fuel combustion and biomass burning.

[7] In this work BC and primary OC emissions from fossil fuel combustion are from Cooke *et al.* [1999]. This inventory places global BC and OC emissions at 5.1 Tg yr^{-1} and 7.0 Tg yr^{-1} , respectively, with a majority of the emissions from coal combustion. The base year for energy consumption and emissions was 1984. It should be noted that in this inventory emission factors for developing countries are enhanced by a factor of five relative to developed countries to account for the lag in the adoption of combustion and pollution control technologies. Most of the Asian countries fall in the developing world category, which results in contributions of 40% and 35% for global fossil fuel BC and OC emissions, respectively. Fossil fuel emissions may vary temporally, but in the absence of information on seasonality, we distribute the annual emissions uniformly throughout the year.

[8] The biomass combustion sources include biomass use for domestic energy (biofuels) and open biomass burning. Open biomass burning sources are crop waste burning in the fields, prescribed forest fires to avoid accidental fires, and accidental forest fires. Forest fires are known to be region specific and take place during the dry season. So any estimation of the emissions from this source must account for the seasonal and interannual variability of the forest fires. In the present study we use biomass combustion emissions from CW96 which include both biofuels and open burning sources. As CW96 do not give the split between these two sources, we apply a spatially distributed ratio of open to total biomass burning emissions from Lioussse *et al.* [1996]. We then estimate the seasonal to interannual variability by combining this source function with satellite-derived fire counts from ATSR (Along Tracking Scanning Radiometer onboard ERS-2 satellite) [Arino *et al.*, 2001]. Emissions are scaled by the ratio of monthly mean to climatological mean fire counts for the period of August 1996 to December 2001 at a resolution of $15^\circ \times 15^\circ$. We are aware of potential biases of the ATSR fire counts caused by pixel size, night time, and clear-sky sampling [Generoso *et al.*, 2003]. Despite these limitations, this approach allows to better represent the interannual seasonality of the open biomass burning emissions [Schultz,

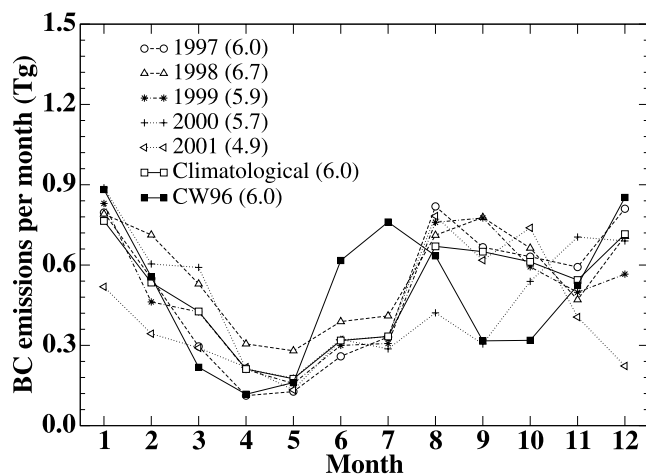


Figure 1. Global black carbon emissions from biomass burning for 1997–2001. The multiyear seasonal BC emissions are constructed by combining CW96 biomass burning emissions with ATSR fire counts (see text).

2002; Duncan *et al.*, 2003]. Generoso *et al.* [2003] also showed that there was an overall good agreement among the various satellite products of fire counts and burned areas.

[9] The OC emissions from all types of biomass burning sources are derived by assuming an OC to BC ratio of 7.0, a value within the range used by Lioussé *et al.* [1996] and Chin *et al.* [2002]. The OC to BC ratio may vary for different biomass types, which introduces some uncertainty in the biomass OC emissions. The OC emission rate must also be multiplied by the ratio of OM to OC to account for other species associated to organic carbon. A value of 1.2–1.4 is usually applied but atmospheric measurements of carbonaceous aerosols during the last decade show that the OM to OC ratio can be up to 2.3–3.2 depending upon the source type and sample location [Turpin and Lim, 2002]. From a review of available in situ aerosol measurements, Turpin and Lim [2002] derive a value of 1.6 and 2.1 for urban and nonurban aerosols, respectively. In light of this new information, we use OM to OC ratio of 1.4 and 1.6 for fossil fuel and biomass combustion, respectively, to convert emission rates of OC to OM. These values, although being larger than those used in previous modeling studies, may still be on the low side.

[10] Global seasonal biomass burning BC emissions for 1997–2001 along with the emissions by CW96 are shown in Figure 1. There is a significant shift in the magnitude and seasonality of the emissions from year to year. The global BC emissions from biomass burning range between 4.9 to 6.7 Tg yr⁻¹ for the different years. As we assume that emissions from biofuels are constant throughout 1997–2001 (at 1.0 Tg yr⁻¹), the interannual variability results only from open burning sources. The global OC emissions from biomass range from 37.5 to 46.9 Tg yr⁻¹ for the period 1997–2001. The variability in carbonaceous aerosol emissions from year to year is therefore about ±15% around the mean at the global scale. However, the variability at regional scales is larger, in particular in South America with a year to year variability of ±30%. During

1997 there was an increased fire activity over Asia resulting in a 60% increase in BC emissions as compared to climatological emissions. As large-scale open burning emissions over Asia account for about 3% of the global emissions, this does not show up much in the global seasonal cycle.

[11] Apart from combustion sources, OC is also produced by natural processes through condensation of volatile organic compounds (VOCs). In this study we only consider secondary OC formation from terpenes. The yield of OC from terpenes is in the range of 0.1–15% and depends on many parameters including initial concentration of terpenes, the hydrocarbon to NO_x ratio, and whether the oxidation is initiated by O₃ or OH. We use a constant yield of 11% for terpene emissions, a value within the range determined by Pandis *et al.* [1991] to estimate secondary OC emissions. The spatial and seasonal distribution of terpene emissions is taken from Guenther *et al.* [1995]. This results in natural OC emissions of 13.9 Tg yr⁻¹. We do not include OC formation from isoprene because the particle yields under ambient conditions are negligible [Pandis *et al.*, 1991]. The production of secondary organic aerosols estimated from global chemical models ranges from 11.2 to 79 Tg yr⁻¹ [Kanakidou *et al.*, 2000; Chung and Seinfeld, 2002; Tsigaridis and Kanakidou, 2003] depending upon the assumed yield factors for different VOCs. In this study, we do not include the secondary OC formation from VOCs released from anthropogenic sources.

[12] Streets *et al.* [2003] recently developed an emission inventory for Asia with 2000 as base year and considering regional combustion technologies and related emission factors. Emissions of carbonaceous aerosols from this inventory are nested into our global emission maps. The global total carbonaceous aerosol emissions from different source types are summarized in Table 1.

[13] Carbonaceous aerosols are predominantly emitted in the hydrophobic form, but some fraction of the emissions may be in hydrophilic form as well [Cachier, 1998]. Various chemical compounds are attached to both BC and OC, which governs their chemical composition as the aerosol ages in the atmosphere. Here, we assume that BC emissions from both fossil fuel and biomass burning occur as 80% hydrophobic and 20% hydrophilic, whereas OM emissions occur as 50% hydrophobic and hydrophilic. The aging process of BC and OM is represented by a transfer of the hydrophobic to hydrophilic form with an exponential lifetime (λ) of 1.63 days, which is close to the value employed by CW96. The transformation from hydrophobic to hydrophilic form is computed using the following equation:

$$\left. \frac{d[BC_{philic}]}{dt} \right|_{tr} = \left. \frac{-d[BC_{phobic}]}{dt} \right|_{tr} = \frac{[BC_{phobic}]}{\lambda} \quad (1)$$

where the *tr* subscript indicates the transformation process.

[14] Open biomass burning emissions are known to be released at higher altitudes due to thermal convection by fires. We therefore emit them in the model layers 3 to 5, corresponding roughly to altitudes of 350 to 1500 m. Over Asia carbonaceous aerosols from fossil fuel combustion in large point sources (e.g., power plants, iron and steel, etc.) are emitted into the model second layer (altitude range of

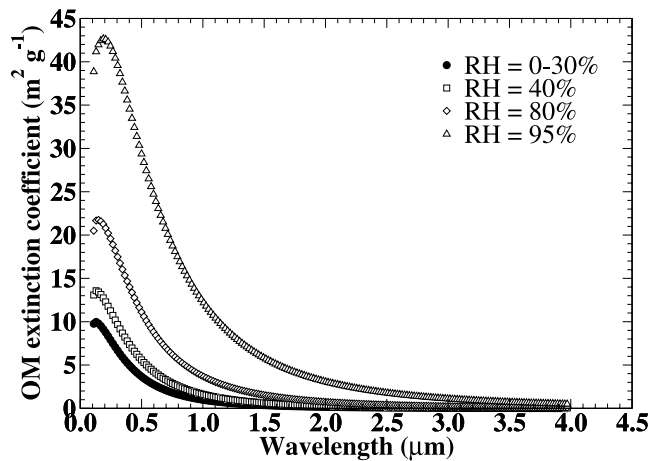


Figure 2. Mass extinction coefficient (m^2g^{-1}) as a function of wavelength for hydrophilic organic matter.

150 to 350 m) while other sources (e.g., transportation, domestic, and small scale industries) are released near the surface.

2.3. Dry and Wet Deposition

[15] The aerosol dry deposition flux to the ground is assumed to be proportional to both the concentration in the lowest model layer and a prescribed dry deposition velocity. Since BC and OM aerosols are assumed to be in the submicron mode, a constant dry deposition velocity of 0.1 cm s^{-1} is used for all surface types, similar to what is done in many of the global models of carbonaceous aerosols [Cooke and Wilson, 1996; Chung and Seinfeld, 2002]. A more appropriate formulation which depends on surface type, type of vegetation, and atmospheric stability is under development. We do not differentiate between the hydrophobic and hydrophilic fractions as far as dry deposition is concerned.

[16] Wet deposition (or scavenging) is treated separately for stratiform and convective rain and differently for the hydrophobic and hydrophilic fractions. For in-cloud scavenging, we apply a parameterization similar to that of Giorgi and Chameides [1986]. The scavenging rate (s^{-1}) is given by

$$W = \beta f r \quad (2)$$

where f is the cloud volume fraction, r is the fraction of the chemical species in the aqueous phase, and β is the rate of conversion of cloudwater to rainwater (in unit of $\text{kg kg}^{-1} \text{ s}^{-1}$). The parameter r is set to 0.7 for hydrophilic BC and OM, similar to sulfate aerosols [Boucher et al., 2002]. This reflects the fact that a fraction of aerosols can be interstitial in clouds as shown by a number of measurements for sulfate and other aerosols [Boucher and Lohmann, 1995; Gillani et al., 1995]. There is no in-cloud scavenging for the hydrophobic fraction of BC and OM (r is set to 0.0).

[17] The parameter β at model level k is computed from the three-dimensional precipitation flux (P_r , stratiform or convective, in $\text{kg m}^{-2} \text{ s}^{-1}$) and a prescribed liquid water

content ($q_l = 0.5$ and 1.0 g kg^{-1} for stratiform and convective clouds, respectively):

$$\beta_k = \frac{P_{r,k} - P_{r,k+1}}{\rho_{\text{air},k} \Delta z_k f_k q_l} \quad (3)$$

where ρ_{air} is the air density (kg m^{-3}) and Δz_k is the thickness of layer k . We do not distinguish between liquid and ice precipitation as far as in-cloud scavenging is concerned.

[18] Below-cloud scavenging is parameterized by integrating over the population of raindrops the volume of space that is swept by a raindrop during its fallout, the expression for the scavenging rate (s^{-1}) is

$$K = \frac{3 P_r \alpha}{4 R_r \rho_{\text{water}}} \quad (4)$$

where R_r is an average raindrop radius (set to 1 mm), ρ_{water} is the water density (kg m^{-3}), and α is the efficiency with which aerosols are collected by raindrops. For the parameter α , we selected a value of 0.001 and 0.01 for raindrops and snowflakes, respectively, based on measurements compiled by Pruppacher and Klett [1997]. Below-cloud scavenging is applied to both hydrophobic and hydrophilic carbonaceous aerosols in the same manner.

[19] Because the three-dimensional precipitation fluxes are available in the GCM, we do not have to assume a vertical profile of precipitation. The release of aerosols at a level k is equal to the amount of the given species which was scavenged at higher levels multiplied by the fraction of precipitation which is evaporated. A multiplicative factor of 0.5 is applied for BC and OM to account for the fact that raindrops can shrink without evaporating totally. In the event of a total evaporation of the precipitation flux, the aerosols are released totally as well.

2.4. Convective Transport

[20] We use the mass fluxes simulated by the Tiedtke [1989] scheme to parameterize convective transport of aerosols. We account for the vertical transport of aerosols in updrafts, downdrafts, and in the environment, and for entrainment and detrainment from and to the environment. The convective transport is performed after the wet scavenging calculation in order to avoid upward transport of material which is necessarily scavenged by precipitation. In addition, we scavenge a fraction of the soluble aerosols released to the environment [Balkanski et al., 1993; Crutzen and Lawrence, 2000; Mari et al., 2000]. This fraction is set to 20% and 50% for the hydrophobic and hydrophilic fractions, respectively. Convective transport is applied in a

Table 1. Summary of Carbonaceous Aerosol Emissions

Source Type	BC, TgC yr ⁻¹	OM, Tg OM yr ⁻¹
Fossil fuels	5.2	15.7
Biomass burning	6.4	73.2
Domestic fuels	1.1	14.5
Open burning	5.3	58.7
Natural	–	19.5
Total	11.6	108.4

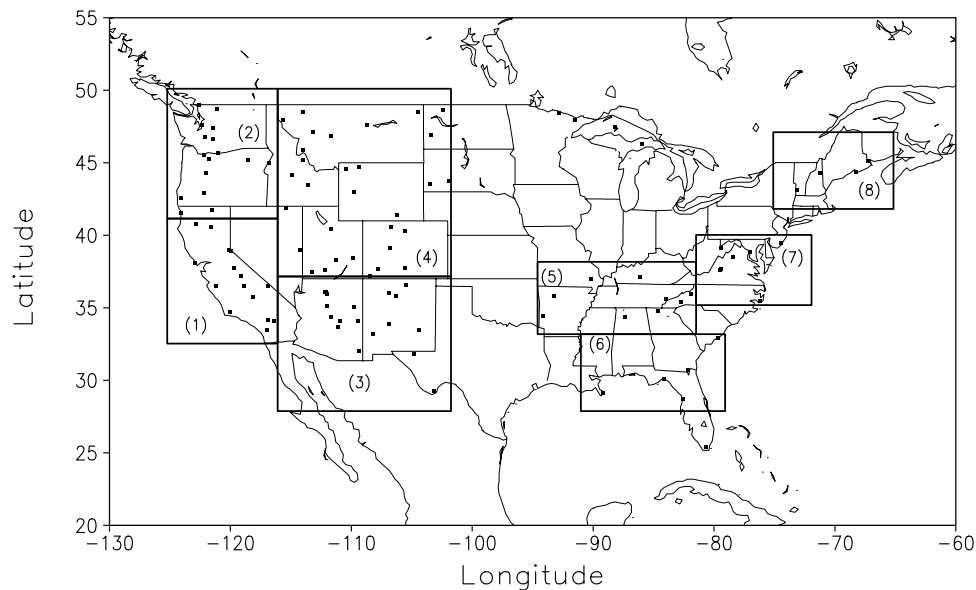


Figure 3. The different regions used in the comparison to IMPROVE data.

bulk manner without distinguishing between the interstitial and the dissolved fractions of aerosols.

2.5. Aerosol Optical Properties

[21] Aerosol optical properties (mass extinction coefficient, single scattering albedo, and asymmetry factor) are computed in the shortwave range from the assumed aerosol size distributions and refractive indices. We assume log-normal size distributions for BC and OM with parameters explicated in Table 2. The size distribution properties for BC are taken from the Global Aerosol Data Set (GADS) [Köpke *et al.*, 1997] and for OM we assume a typical size distribution similar to that of sulfate aerosols [Boucher and Anderson, 1995]. The refractive indices for the dry BC and OM are from Köpke *et al.* [1997]. Black carbon and the hydrophobic fraction of OM are assumed not to grow in size with relative humidity (RH). It is generally considered that aged OM is hydrophilic and mostly scattering. In the absence of reliable data, we use for OM the hygroscopic growth of ammonium sulfate calculated from Tang and Munkelwitz [1994]. The refractive index for hydrophilic OM as a function of RH is calculated as the volume weighted average of the refractive indices of water and OM (Lacis *et al.*, Parameterization of relative humidity effects of hydrophobic aerosols in a climate GCM, http://gacp.giss.nasa.gov/data_sets/lacis/database.html). Treating water uptake of OM like sulfate aerosols is considered to be an upper limit since all organic compounds may not be as soluble as ammonium sulfate. The mass extinction coefficient for hydrophilic OM increases substantially at large RH (Figure 2). The mass extinction coefficients for BC and OM at $0.55\ \mu\text{m}$ computed here lie in the range of reported values in the literature (Table 2).

2.6. Simulations

[22] Simulations are carried out in nudged mode [Haughustaine *et al.*, 2004]. Horizontal model winds are nudged to 6-hourly wind fields from the European Centre for

Medium Range Weather Forecasts (ECMWF) with a relaxation time of 0.1 days. The simulations are carried out for the period January 1997 to December 1999, after allowing for a 4 month spin-up period. This ensures that the simulated transport is reasonably constrained by ECMWF meteorology while the rest of the dynamical and physical processes are driven by the model parameterizations.

3. Model Validation

3.1. Strategy

[23] In this section we compare the model predicted concentrations of BC and OC with measured ones at different geographical locations. The comparisons are made over the regions of North and South America, Europe, Asia, and Africa. However, the number of measurements available is limited and some are made over short periods of time. For this model evaluation we use the measured mass concentrations of BC wherever they are available. At some stations (Barrow, Sable Island, and Mauna Loa) measurements are reported as aerosol absorption. These are converted to BC mass concentrations using an absorption coefficient of $7.44\ \text{m}^2\text{g}^{-1}$ at 550 nm, consistently with the values given in Table 2. As pointed out by Lioussé *et al.* [1993], BC mass absorption coefficient varies over a wide range ($4\text{--}16\ \text{m}^2\text{g}^{-1}$) depending upon the source type and transport history, which could introduce some uncertainty in the comparison. In case of OC measurements are very sparse, which makes it more difficult to evaluate the model. Since we do not treat OM from fossil fuel and biomass burning separately in the model, we cannot convert back OM to OC concentrations in a rigorous manner. We instead apply the OM to OC ratios of 1.4 and 1.6 in regions dominated by fossil fuel and biomass sources, respectively. In Asia sources from fossil fuel and biomass burning are equally important and we use an average OM to OC ratio of 1.5. In Africa and Central and South America the major source of aerosols is from biomass burning. To validate the model in these

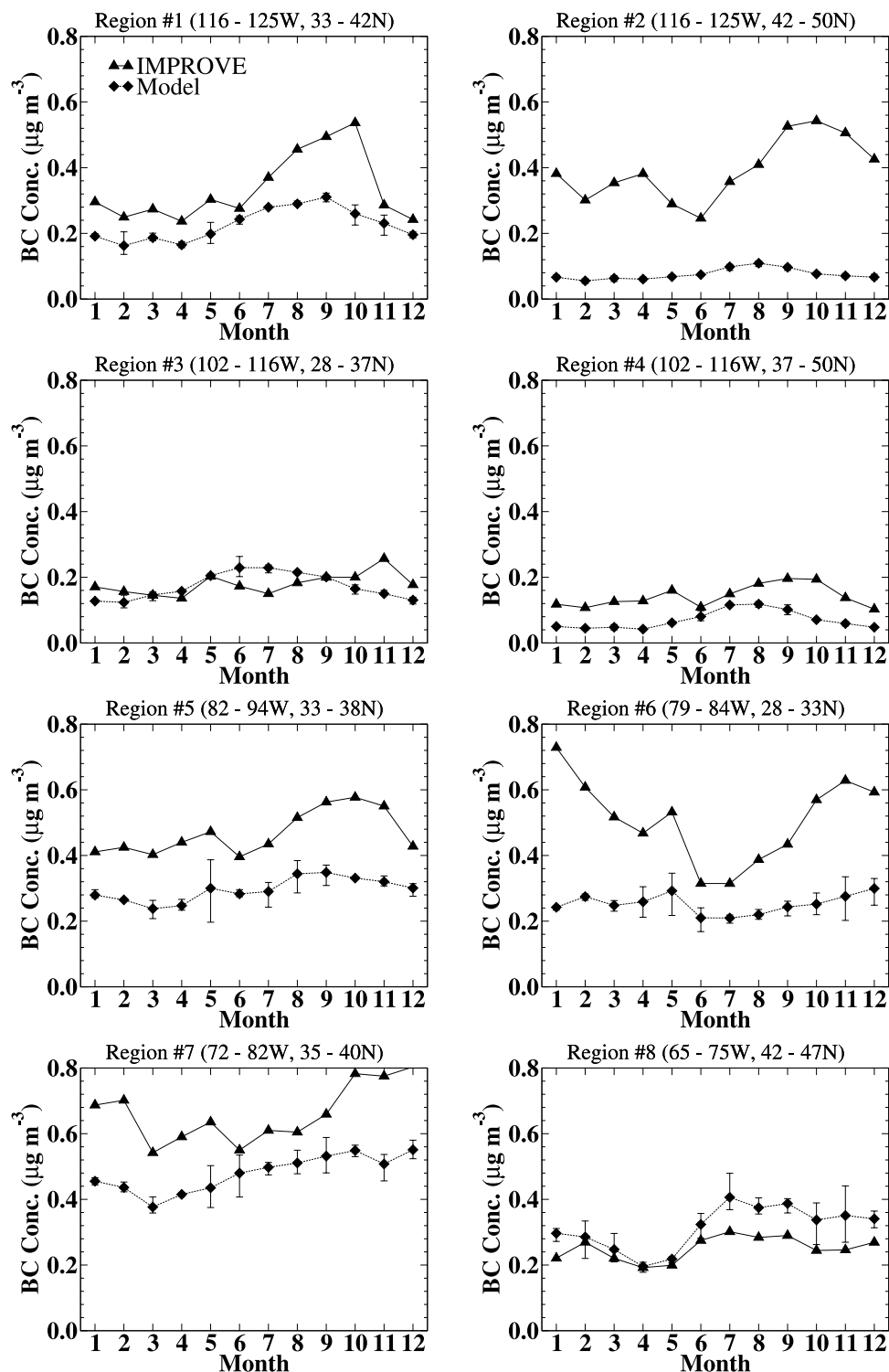


Figure 4. Comparison of model predicted BC concentrations with IMPROVE measurements over the United States. The measurements and model predicted values are averaged for the period 1997–1999. Maximum and minimum monthly mean values during 1997–1999, which constitute a range in the model estimates, are also shown.

regions we also compare the simulated and measured AODs at 670 nm.

3.2. North America

[24] A detailed database of carbonaceous aerosol measurements has been made available over the United States

from the Interagency Monitoring of PROtected Visual Environments (IMPROVE) program [Malm *et al.*, 2000]. Most of the IMPROVE stations (~ 150) are located in national parks or protected areas and are therefore expected not to be influenced by urban sources. The IMPROVE sampling strategy consists of taking twenty-four

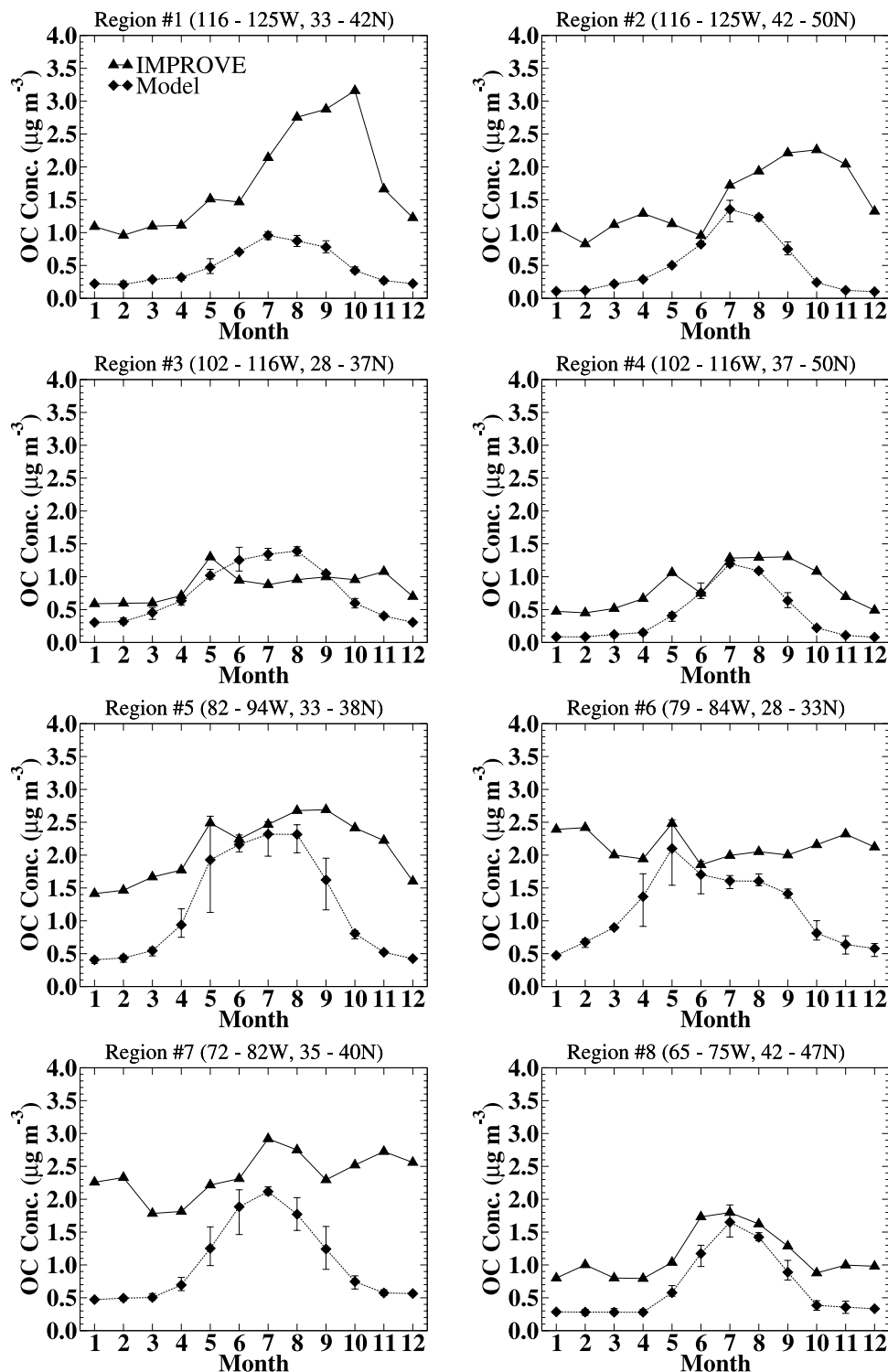


Figure 5. Same as Figure 4, but for OC.

hour samples twice a week on Wednesdays and Sundays. Comparing model results at a resolution of $3.75^\circ \times 2.50^\circ$ with point measurements could be a problem as the measurements are often affected by local sources and transport patterns not resolved in a global transport model. To avoid this, we first interpolate all available measurements for the period of 1997–1999 to a $1^\circ \times 1^\circ$ grid. We then divide the United States into eight regions

clustering the monitoring stations and average spatially the concentrations for each month (see Figure 3). The model concentrations are also sampled following the IMPROVE sampling strategy for all the years (1997–1999) and are spatially averaged over the same regions and time as the measurements. We believe that this procedure allows a more fair evaluation of a large-scale model with observations.

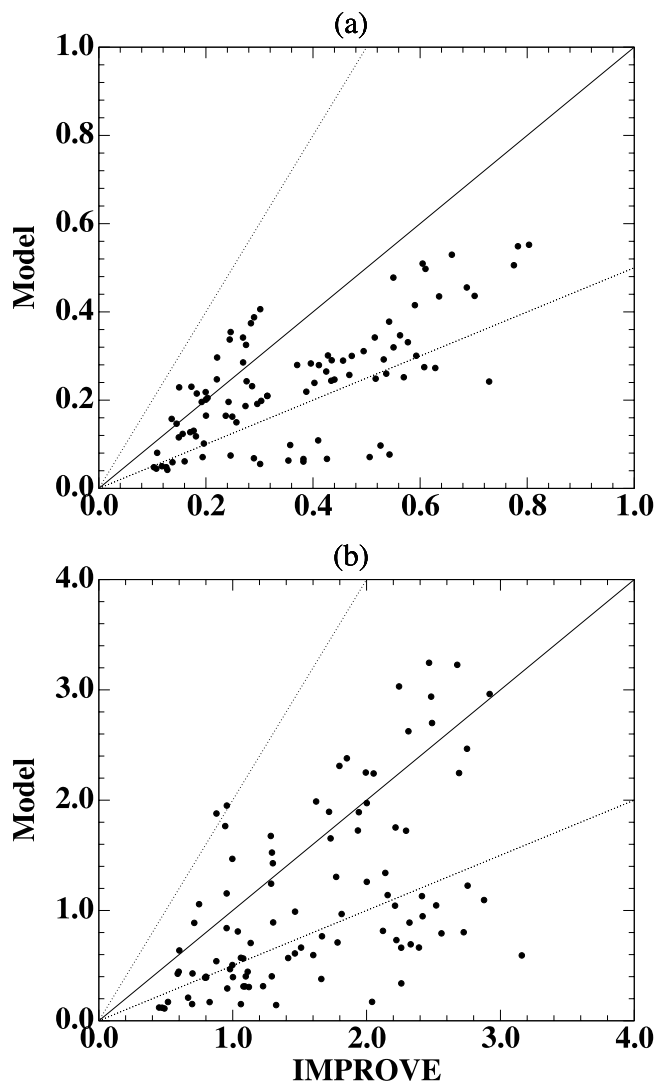


Figure 6. Scatterplot between IMPROVE and modeled monthly mean concentrations for (a) BC, as presented in Figure 4 and (b) OC, as presented in Figure 5. The solid line is the 1:1 line, while the dotted lines are the 1:2 and 2:1 lines.

[25] The comparison between the modeled and IMPROVE BC and OC concentrations is shown in Figures 4 and 5. Despite the fact that fossil fuel emission sources are constant throughout the year, there is a general agreement between the simulated and measured seasonality in concentrations, which places some confidence in the model skills. Aerosol concentrations over the regions on the west coast are primarily influenced by fossil fuel sources and have negligible interannual variability because of constant emission sources throughout the simulation period. Regions on the east coast in addition to local fossil fuel emissions also receives biomass burning plumes from Africa and have an interannual variability about 10–30% especially during biomass burning season (Figures 4 and 5). The correlation coefficient between IMPROVE and modeled BC concentrations is 0.67 with 73% of the data points falling within a factor of 2 (Figure 6a). The remaining 27% of the data points are underestimated by

the model, especially over the west coast of the United States. The OC concentrations are underpredicted by a factor of 2 to 5 depending on the region under consideration. The correlation coefficient between IMPROVE and modeled OC concentrations is 0.54, with only 50% of the data points falling within a factor of 2 (Figure 6b). The interannual variability in the simulated concentrations could not explain the discrepancy between the observations and modeled concentrations. The underprediction seems to be a common feature of global models [Cooke *et al.*, 2002; Chung and Seinfeld, 2002] as well as regional models [Park *et al.*, 2003]. Among the plausible reasons for this underprediction are the absence of anthropogenic secondary OC source and/or too low OC emissions in the model over North America. In a recent study, Cooke *et al.* [2002] doubled OC sources from fossil fuel sources to account for secondary OC production in the atmosphere. Despite this additional source OC concentrations in Cooke *et al.* [2002] remain underestimated by a factor of 2 in comparison to IMPROVE measurements. Chung and Seinfeld [2002] introduced a detailed scheme for secondary OC formation, but also underestimate OC concentrations by a factor of 2 to 10 at individual sites. Altogether this suggests that underestimation of primary OC emissions over North America could be the major reason for the model underprediction of OC concentrations. Updated gridded emission inventories of BC and OC are therefore very much needed over North America.

3.3. Europe

[26] Available carbonaceous aerosol measurements over Europe for the last decade (between 1991 and 2000) were compiled by Putaud *et al.* [2002]. Monitoring stations, with continuous measurements for at least 6 weeks in one season, were classified as background, rural, near city, and urban, as per the criteria of the European Environmental Agency. The global transport models are not expected to represent the measurements at urban locations and we have not included comparison for these sites. The seasonally averaged concentrations of BC and OC for rural and background stations are shown in Figure 7. It may be noted that measurements at various sites were taken during 1991–2000. The time period of measurements for some of the stations overlaps with simulation period (1997–1999), while for other stations it is either pre-1997 or post-1999. Analytical methods and number of samples also differ from station to station. Modeled BC and OC concentrations at rural sites fall within a factor of 2 of measurements. At background sites only BC measurements are available and predicted concentrations are biased toward lower values. A comparison of seasonal concentrations at other sites in Europe is shown in Figure 8. These sites primarily influenced by fossil fuel sources and have smaller than 10% of variation in monthly mean concentrations among different simulation years. The model underestimates both BC and OC concentrations at Helsinki throughout the year by a factor of 2 to 3 (Figures 8a and 8b). At Krvavec the model agrees well with the measured BC concentrations throughout the year (Figure 8c).

3.4. Asia

[27] Available measurements of carbonaceous aerosols over Asia are sparse and, most of the time, they are for a

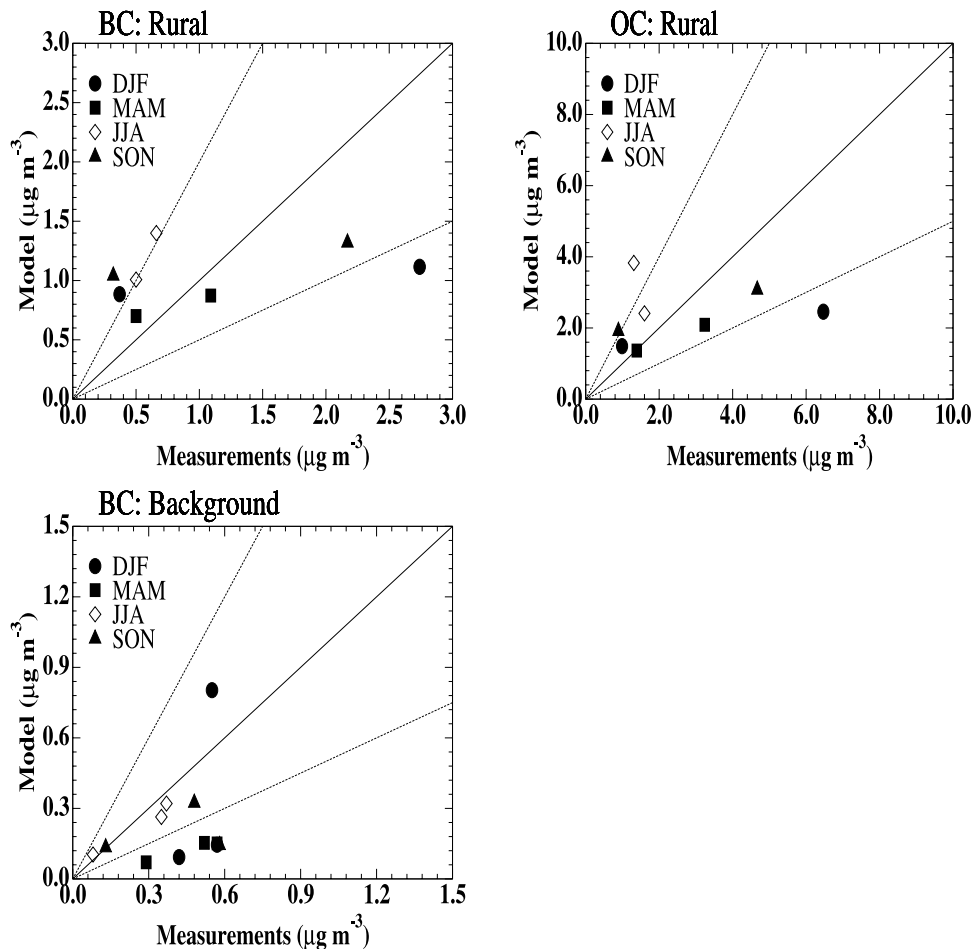


Figure 7. Modeled and observed BC and OC concentrations at different locations over Europe. Measurements are from the compilation of *Putaud et al.* [2002], and modeled values are for the period 1997–1999. The solid line is the 1:1 line, while the dotted lines are the 1:2 and 2:1 lines.

short time period in urban areas. In South Korea measurements of carbonaceous aerosol were carried out at Kosan, Kangwha, Sihwa, and Chongju between 1994 and 1999 [Kim *et al.*, 2000; Lee and Kang, 2001; Park *et al.*, 2001]. These measurements are semi-continuous and modeled concentrations are also sampled for the reported sampling periods for the three years (1997–1999) and averaged (Figure 9). On the one hand the BC concentrations are smaller than $1.5 \mu\text{g m}^{-3}$ and are overestimated in the model by a factor of 2–5 at Kosan. On the other hand the measured BC concentrations are highest ($3\text{--}7 \mu\text{g m}^{-3}$) and are underestimated by the model by a factor of 2–4 at Chongju. At Kangwha and Sihwa the concentrations fall within a factor of 2. The model OC concentrations at all four sites fall within a factor 2, with a bias toward smaller values. A comparison of modeled and measured BC and OC concentrations for other locations in Asia is shown in Figure 10. The model fails to reproduce the measured large BC and OC concentrations at both urban sites of Sapporo and Uji (Figure 10).

3.5. Remote Locations

[28] Remote locations are by definition not influenced by nearby sources, which allows a test of the model transport and deposition parameterizations. Comparison of modeled

BC concentrations with long-term measurements at remote locations in the Northern and Southern Hemispheres is shown in Figure 11. The long-term concentrations at Barrow, Sable Island, and Mauna Loa are taken from the Climate Modeling and Dynamics Laboratory (CMDL) monitoring network. We have sampled the model BC concentrations days for which absorption measurements are reported during the 1997–1999 and monthly averaged. For other remote locations (Jungfraujoch, Amundsen-Scott, and Halley) we use measurements reported in the literature.

[29] The Barrow, Alaska site is representative of the Arctic region. During winter it is characterized by a strong vertical temperature gradient, resulting in a stratification near the surface and the formation of a shallow boundary layer with an accumulation of aerosols near the surface. Large-scale models do not have the capability to resolve this phenomenon because of a coarse vertical resolution in the planetary boundary layer. This results in a drastic underestimation of aerosol concentrations during the winter season, common to other global models [Lioussé *et al.*, 1996; Chung and Seinfeld, 2002]. A comparison of modeled and measured concentrations at Sable Island, Nova Scotia is shown in Figure 11b. The model underestimates the concentrations by a factor of 3 to 6 throughout the year, which may be due to too low emissions upwinds of Sable

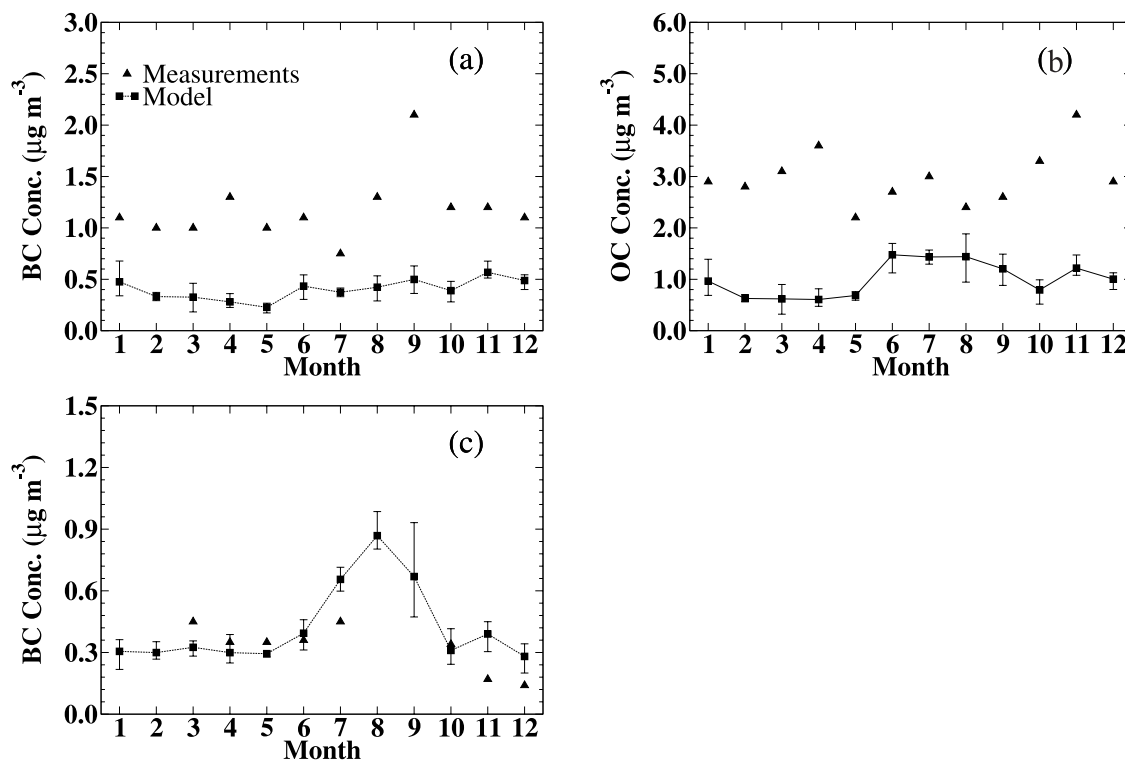


Figure 8. Modeled and observed concentrations in Europe at Helsinki (60.3°N, 24.9°E) for (a) BC and (b) OC and at Krvavec (46.3°N, 14.5°E, 1740 m asl) for (c) BC only. The measurements for Helsinki and Krvavec are from *Vidanoja et al.* [2002] and *Bizjak et al.* [1999], respectively. Maximum and minimum monthly mean values during 1997–1999, which constitute a range in the model estimates, are also shown.

Island or too efficient scavenging of the aerosols. It should be noted that emissions from boreal fires are not included in our model.

[30] Jungfraujoch, Switzerland is a free-tropospheric site, located in the mountain range of the Alps. The observations show a peak concentration in July and a secondary peak in April (Figure 11c). The seasonal cycle observed at this site results from the vertical transport of boundary layer air

masses from the Swiss Plateau [*Baltensperger et al.*, 1997]. Model concentrations are in reasonable agreement with observations in terms of order of magnitude. The model exhibits a peak in August, i.e., with a one month delay compared to observations. Mauna Loa, Hawaii is also a tropospheric site in the Pacific Ocean (Figure 11d), and the monthly mean model predicted BC concentrations agree reasonably with the measurements (i.e., within a factor of 2).

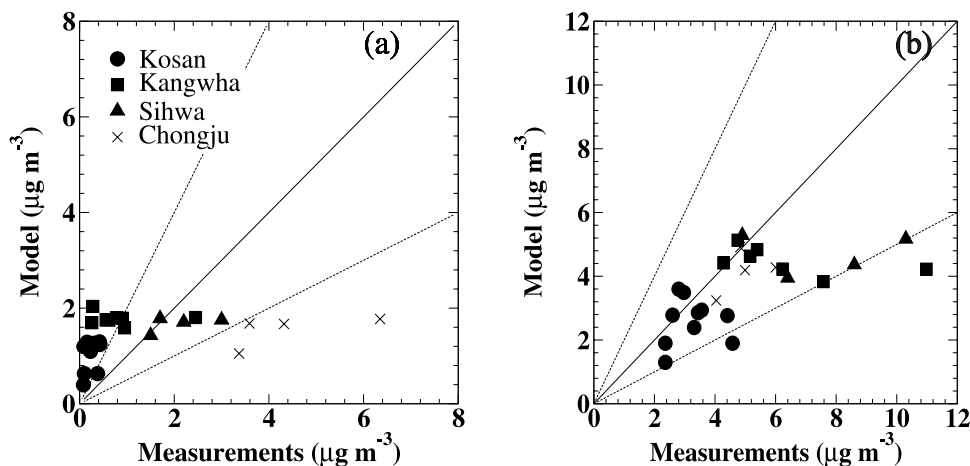


Figure 9. Modeled and observed concentrations of (a) BC and (b) OC at the locations of Kosan (34.0°N, 126.0°E), Kangwha (37.7°N, 126.5°E), Sihwa (37.3°N, 126.7°E), and Chongju (36.7°N, 127.5°E), South Korea. The solid line is the 1:1 line, while the dotted lines are the 1:2 and 2:1 lines.

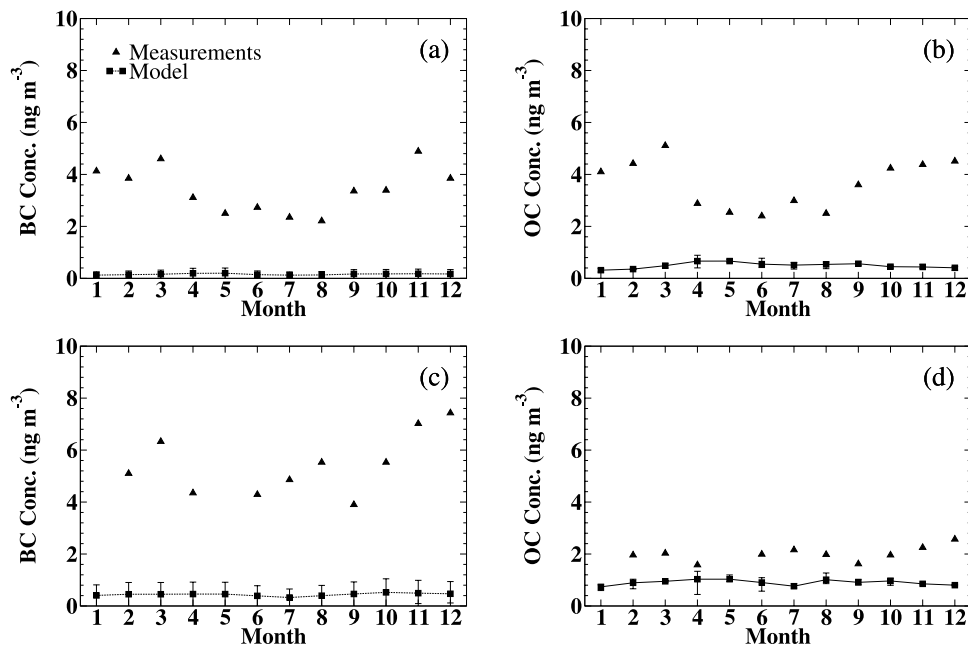


Figure 10. Modeled and observed concentrations of carbonaceous aerosols at Spporo, Japan (43°N , 141°E) for (a) BC and (b) OC, and Uji, Japan (37.3°N , 126.7°E) for (c) BC and (d) OC. Measurements at Sapporo and Uji are from Kaneyasu *et al.* [1995] and Höller *et al.* [2002], respectively. Maximum and minimum monthly mean values during 1997–1999, which constitute a range in the model estimates, are also shown.

In contrast to the continental stations at these remote stations variation in the monthly concentrations among different years is as large as 50%. At these locations the discrepancy between the model and observations during high pollution periods is explained by the interannual variability in the modeled concentrations.

[31] Long-term BC concentrations at Amundsen-Scott and Halley in Antarctica are compared with model estimates in Figures 11e and 11f. The measured BC at these sites comes from long-range transport originating from biomass burning. The measured values are 1 to 2 orders of magnitude smaller than those of previous stations. Although the model underestimates the concentrations by up to a factor of 4 in some months, it simulates values of the right order of magnitude. The modeled concentrations during the biomass burning season vary by a factor of 2 and have close agreement with observed values some of the years compared three years mean values. This may be due to differences in the time periods of observations and model estimates (observations are long-term measurements for the early 1990s whereas the model concentrations are three year averages for 1997–1999). Note that the BC concentrations were inferred from light absorption measurements, which introduces some uncertainty in the comparison as discussed earlier.

[32] The comparison of BC concentrations downwind of Africa at Amsterdam Island and Piton Textor, La Réunion Island is shown in Figure 12. At Amsterdam Island there is a good agreement in the seasonality of the concentrations between the observations and the model. The summer peak in BC concentrations results from increased biomass burning in Africa and is reproduced by the model. At Piton Textor, the seasonal cycle in the BC concentrations is also

well represented by the model with a large peak in summer. It may be noted that the model is able to capture the gradient in concentrations between these two stations downwind of biomass burning sources. The variation in the monthly mean concentrations for the simulation period at Amsterdam Island is larger than that at Piton Textor. However, the variability in the simulated concentrations could not explain the shift in the seasonality between the model and measurements.

3.6. Africa

[33] Likewise biomass burning largely contributes to aerosol concentrations and resulting AODs in Central and Southern Africa. Time series of model predicted AOD from carbonaceous aerosols for the period of 1997–1999 is compared with AERONET measured AOD at 670 nm for various sites in Africa (Figure 13). The model estimates are filtered with daily mean AERONET measurements. Except Mongu other AERONET stations lack the data for the full time period. The model predicted AODs show a agreement in the seasonality compared to observations but with a low magnitude (up to a factor of 3 too low). However, the variability in the observations and model estimates are large and most of the time standard deviations in monthly means overlap with each other. Model emissions may well be underestimated but it should also be kept in mind that AERONET measurements are for daytime, cloud-free conditions, while model AODs are for 24-hour all-sky conditions. Since biomass burning is thought to occur more at day than at night, this may introduce some biases in the comparison. Discrepancies between the modeled and observed AOD may also arise from the additional uncertainties in RH

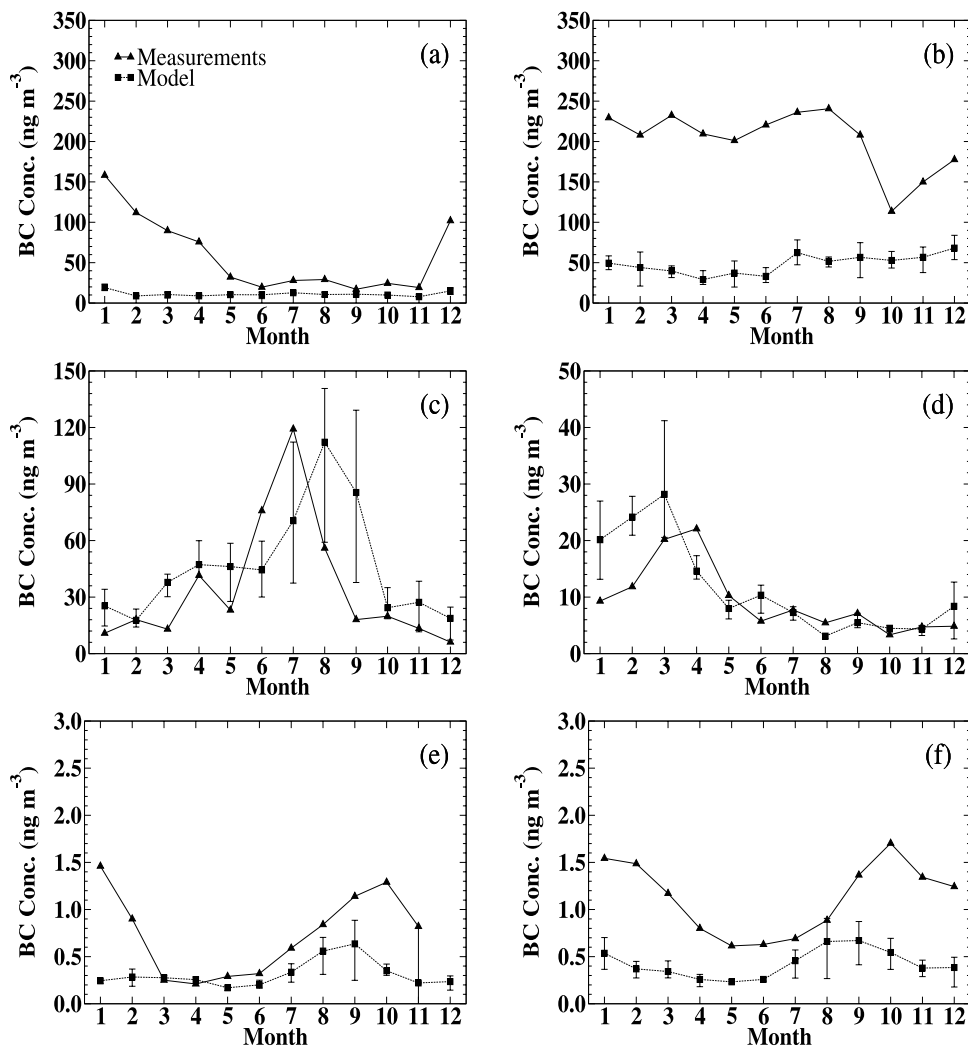


Figure 11. Comparison of measured and modeled BC concentrations at various remote stations: (a) Barrow Alaska (71.2°N, 156.3°W), (b) Sable Island, Nova Scotia (43.9°N, 60.0°W), (c) Jungfrauoch, Switzerland (46.5°N, 9°E, 3454 m asl), (d) Mauna Loa, Hawaii (19.3°N, 155.4°W, 3400 m asl), (e) Amundsen-Scott, Antarctica (89°S, 102°W), and (f) Halley, Antarctica (75.6°S, 26.2°W). Measurements at Barrow, Sable Island, and Mauna Loa are from CMDL aerosol absorption measurements, Jungfrauoch are from *Nyeki et al.* [1998], and Halley are from *Wolff and Cachier* [1998]. Maximum and minimum monthly mean values during 1997–1999, which constitute a range in the model estimates, are also shown.

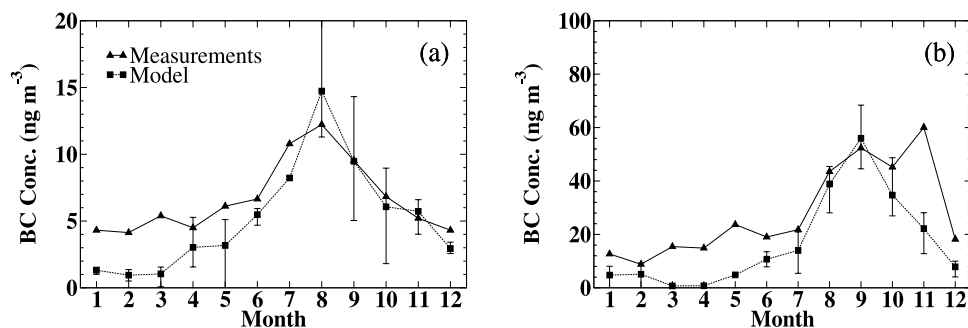


Figure 12. Measured and modeled BC concentrations downwind of Africa at (a) Amsterdam Island (38°S, 77°E) and (b) Piton Textor, La Réunion Island (12.4°S, 55.5°E, 2150 m asl). Measured values for Amsterdam Island and Piton Textor are from *Wolff and Cachier* [1998] and *Bhugwant et al.* [2001], respectively. Maximum and minimum monthly mean values during 1997–1999, which constitute a range in the model estimates, are also shown.

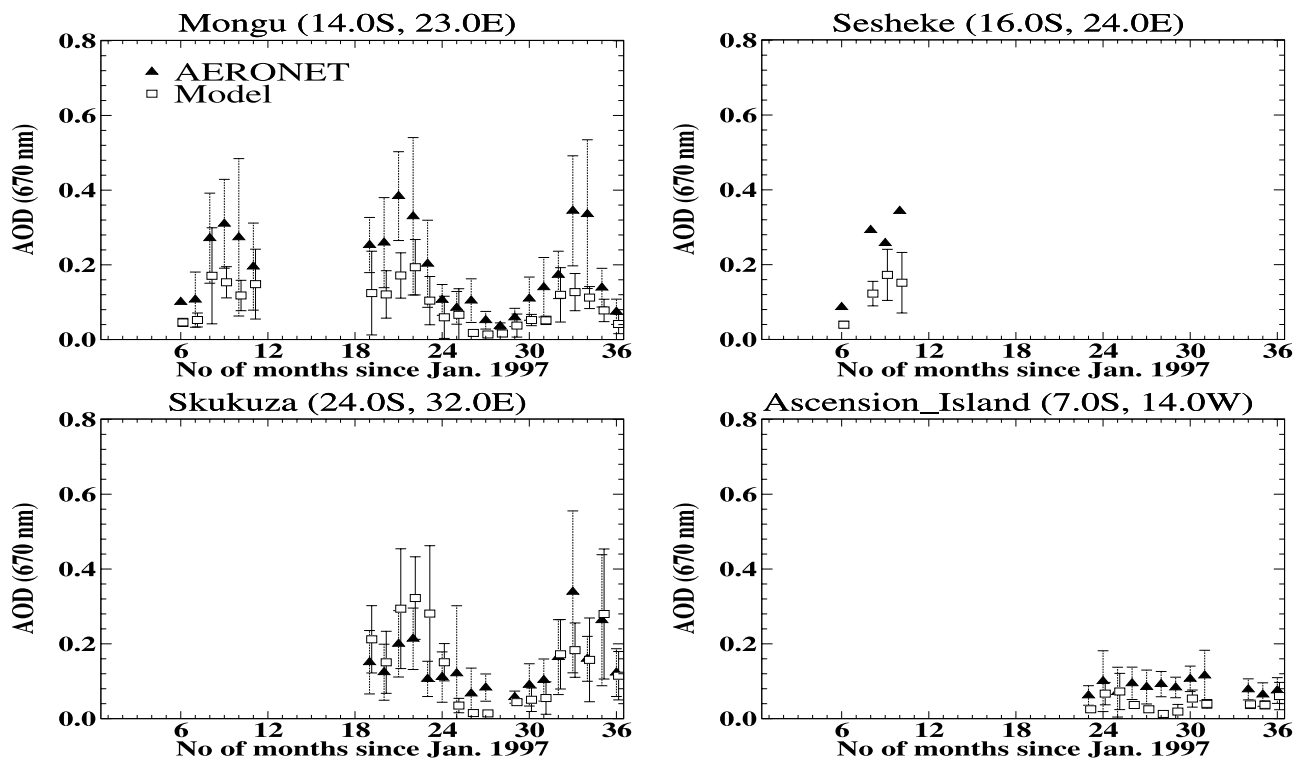


Figure 13. Time series of measured and modeled AOD (at 670 nm) at various locations in Africa. The model values are sampled only days for which AERONET retrievals are available during 1997–1999. The error bar signifies \pm one standard deviation of the daily means around the monthly mean.

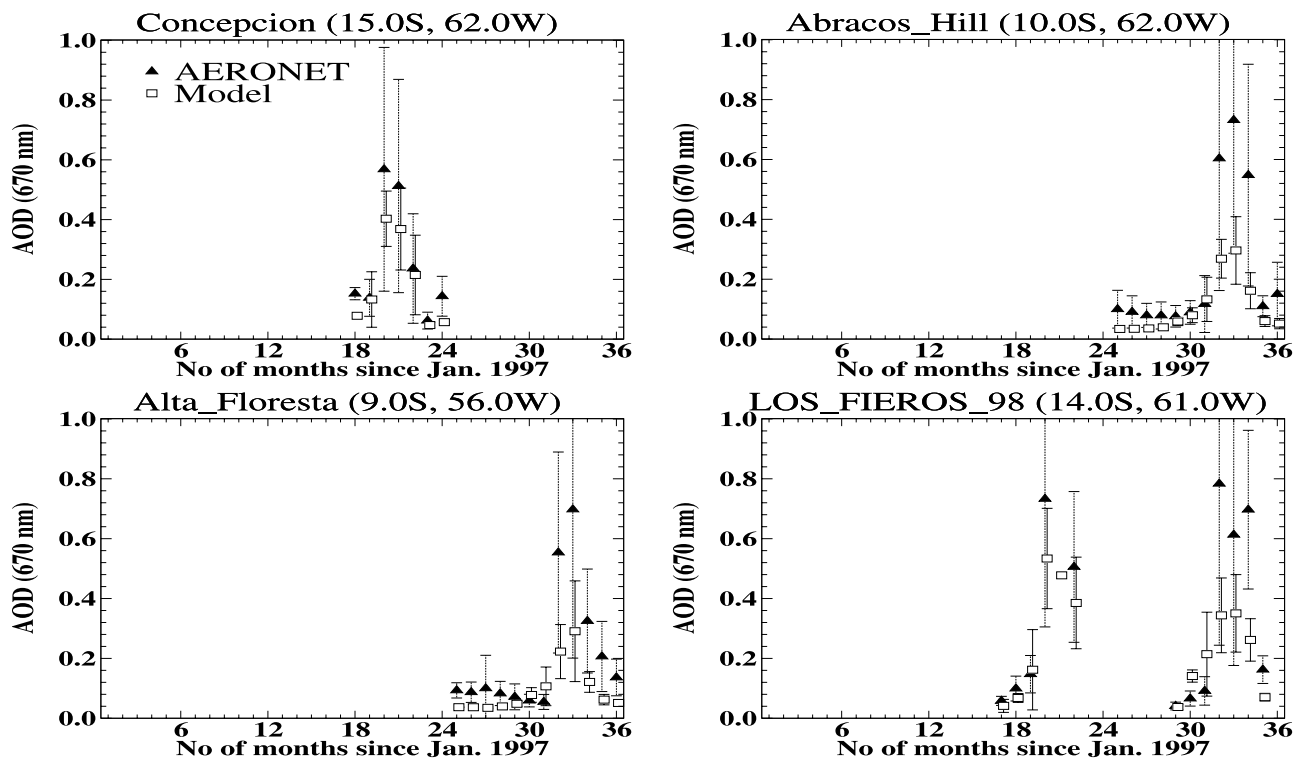


Figure 14. Same as Figure 13, but at locations in South America.

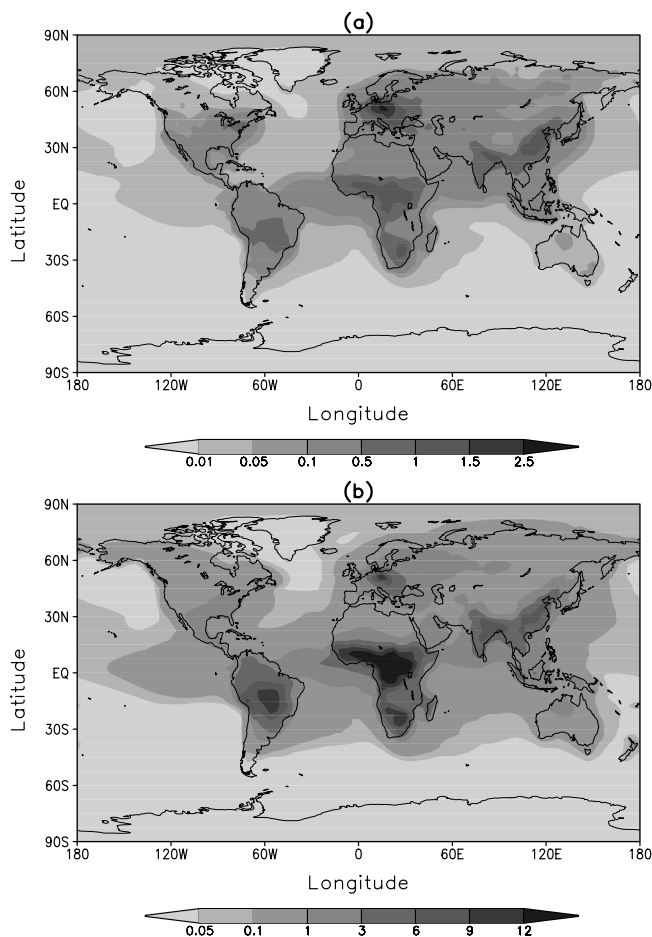


Figure 15. Global distributions of annual mean (a) BC and (b) OM surface mass concentration ($\mu\text{g m}^{-3}$). See color version of this figure in the HTML.

and aerosol growth rate with RH. The correlation coefficient between AERONET and model AODs for all of the sites is 0.70. The mean model AOD (0.085) is 1.6 times lower than the AERONET mean AOD (0.134).

3.7. South America

[34] Carbonaceous aerosols in South America originate mostly from biomass burning. A comparison between model predicted carbonaceous AOD and AERONET measured AOD at 670 nm for various sites in South America is shown in Figure 14. The seasonal cycle in the measurements is reproduced reasonably well by the model with an underestimation of peaks in AOD by a factor of 2–3 during the burning season (mostly September, October, and November). The nonavailability of AERONET data for entire simulation period prevents us from performing a more comprehensive statistical analysis. The correlation coefficient between AERONET and model AODs is 0.88; the model mean value (0.084) is 1.94 times lower by than the AERONET mean value (0.164). Although emissions from biomass burning have been scaled with ATSR fire counts, peak values occur at different months in the model and measurements. *Generoso et al.* [2003] compared different data sets and found differences of up to 2–3 months for the month of maximum fire counts or

burned areas. Improvements in the seasonal cycle of emissions are therefore needed for this region.

4. Global Distributions

4.1. Mass Concentrations

[35] The global distributions of BC and OM concentrations at the surface are shown in Figure 15. The largest BC concentrations are found in the source regions over the continents, especially in eastern Europe, Africa, and Asia. The transport of biomass burning emissions from Africa and South America to the Atlantic and Pacific Oceans is also highlighted. The annually averaged BC burdens are 0.59 and 0.31 mg m^{-2} over the NH and SH, respectively. The largest OM concentrations at the surface (above 12 $\mu\text{g m}^{-3}$) are predicted near the source regions over Africa and South America. Concentrations as large as 9 and 6 $\mu\text{g m}^{-3}$ are also estimated over eastern Europe and Asia, respectively. The hemispheric average OM burdens are 5.01 and 3.66 mg m^{-2} for the NH and SH, respectively.

[36] The annually and zonally averaged concentration of BC is shown in Figure 16a with maxima at the surface in the tropical regions and the northern midlatitudes. Emissions from large scale open biomass burning are injected at higher altitudes, which results in concentrations of 90 ng m^{-3} up to 600 hPa. At midlatitudes in both hemispheres, the

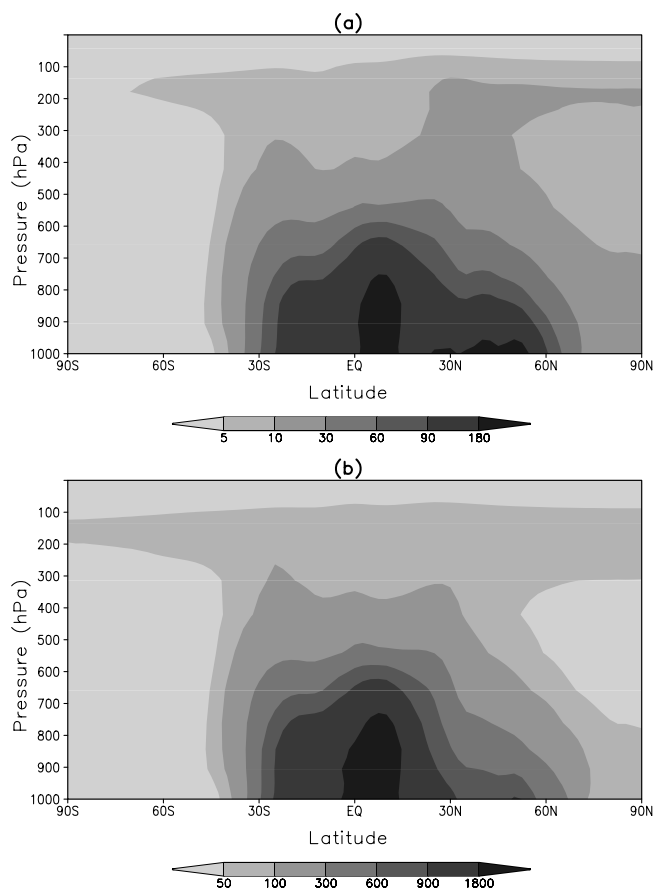


Figure 16. Distribution of the zonal and annual mean (a) BC and (b) OM mass concentration (ng m^{-3}). See color version of this figure in the HTML.

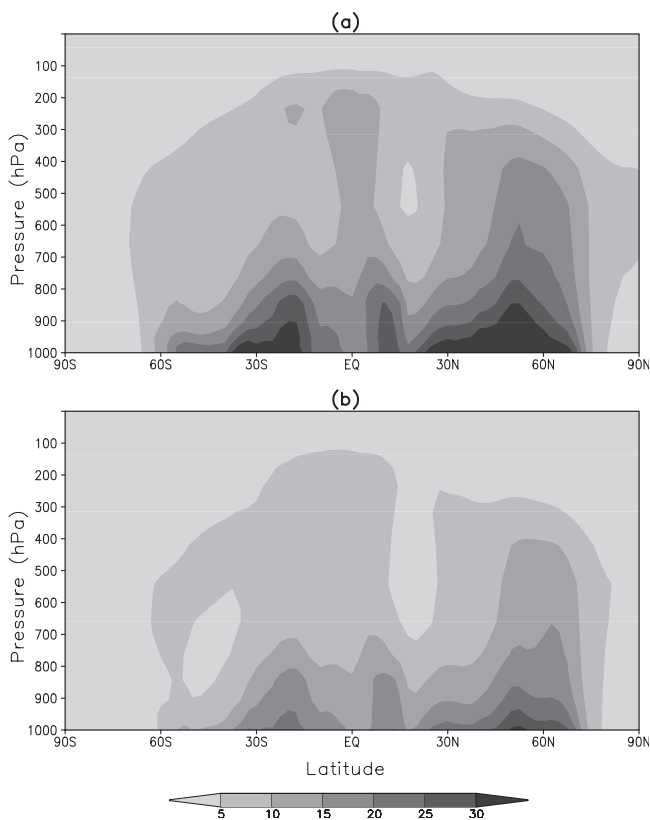


Figure 17. Fraction (%) of (a) BC and (b) OM concentration which is in the hydrophobic mode in zonal annual mean. See color version of this figure in the HTML.

hydrophobic fraction accounts for more than 30% of BC in the lower troposphere (Figure 17a). The fraction of hydrophobic to total BC is largest in the source regions and drops sharply away from the source regions. Above 700 hPa, the contribution of hydrophobic BC is generally less than 15% as most of the BC has been transformed to hydrophilic form. The zonally averaged OM concentration exhibits a peak over the tropical regions, where most of the emissions take place (Figure 16b). Hydrophobic OM contributes up to 20% of the total OM concentrations in the source regions and this contribution decreases rapidly as we move away from the sources (Figure 17b). The fraction of hydrophobic material is less than for BC because only 50% of the OM is emitted in hydrophobic form, instead of 80% for BC.

4.2. Aerosol Optical Depth

[37] Aerosol optical depth for BC and OM is computed using the simulated three-dimensional concentrations and prescribed aerosol optical properties (section 2.5). In the visible (at $0.55 \mu\text{m}$) BC contributes primarily to absorption, therefore the distribution of absorption optical depth (Figure 18a) shows the same patterns as that of the BC burden (not shown), with peak values over and around intense source regions (i.e., Africa, South America, eastern Europe, South and East Asia). The aerosol extinction optical depth is dominated by OM and associated water with largest values, up to 0.25 in annual mean, over Africa (Figure 18b).

The globally and annually averaged AOD from BC and OM is 0.0043 and 0.0258, respectively.

5. Budgets

[38] The global and annual mean BC and OM budgets for the period 1997 to 1999 are summarized in Table 3, along with those from other global models. The estimated BC burden is 0.24 Tg. Wet deposition is the dominant removal mechanism, accounting for 84% of the sink, while dry deposition accounts for the remaining 16%. A majority of the atmospheric burden is contributed by hydrophilic BC (83% or 0.20 Tg) with the complement from hydrophobic BC (17% or 0.04 Tg). Although 80% of total BC is emitted in hydrophobic form only 9% is removed in hydrophobic form through dry and wet deposition, the remaining being converted to hydrophilic BC. This results in a residence time of 1.6 days for hydrophobic BC. Our BC burden of 0.24 Tg lies in the reported range of 0.13–0.32 Tg. The residence time of BC is 7.6 days and lies in the upper end of reported values in the literature (4.0–6.4 days).

[39] The global OM burden is 2.21 Tg. Applying an average OM to OC ratio of 1.5, this corresponds to an

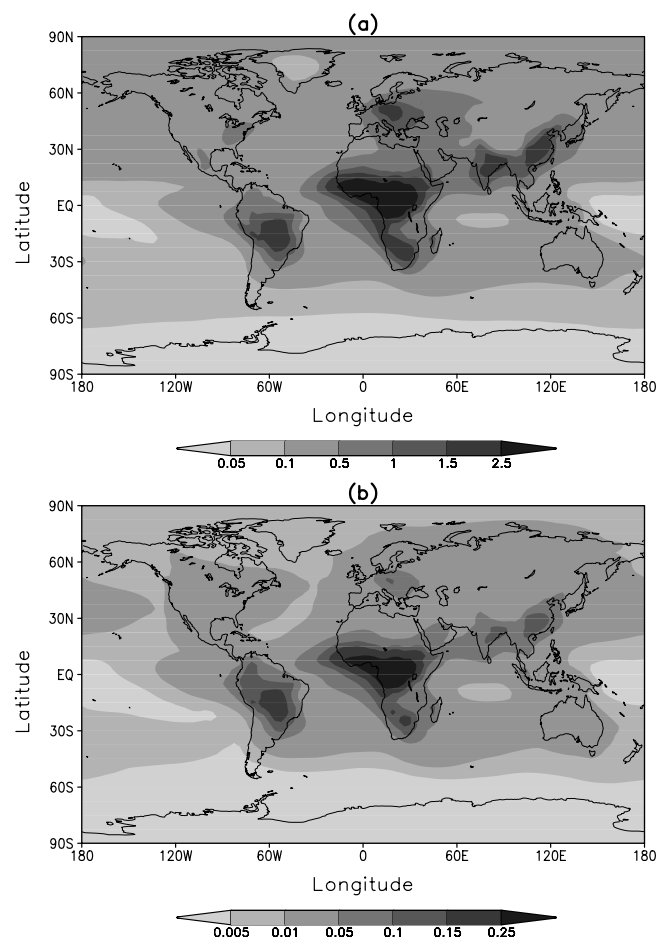


Figure 18. Global distribution of the annual mean (a) absorption ($\times 100$) and (b) extinction AOD at $0.55 \mu\text{m}$ from carbonaceous aerosols. See color version of this figure in the HTML.

Table 2. Physical and Optical Properties (at 0.55 μm) of Dry Carbonaceous Aerosols^a

Aerosol Type	ρ , g cm^{-3}	r_0 , μm	σ_g	Refractive Index	α_e , m^2g^{-1}	ω	g
BC	1.0	0.0118	2.0	1.75 – 0.45 <i>i</i>	9.41	0.21	0.34
OM	1.8	0.0355	2.0	1.53 – 0.005 <i>i</i>	3.16	0.97	0.61

^aHere ρ , dry density; r_0 , modal radius; σ_g , geometric standard deviation; α_e , mass extinction coefficient; ω , aerosol single scattering albedo; g , asymmetry factor.

OC burden of 1.47 Tg, in the range of reported values (0.73–1.5 Tg). The hydrophobic and hydrophilic fractions constitute 10 and 90% of the OM burden, respectively. Hydrophobic OM has a residence time of 1.4 days close to that of hydrophobic BC (1.6 days). The residence time of OM is 7.4 days, slightly larger than other reported values (3.9–6.4 days). Aerosol burden and residence time are sensitive to the assumed percentage of emissions emitted in hydrophobic form and details of the wet scavenging scheme. For example *Lioussse et al.* [1996] assumed that all of the BC emissions were hydrophilic, which resulted in a more effective wet removal and a lower burden of 0.13 Tg. *Koch* [2001] studied the effect of the in-cloud convective scavenging scheme on residence time and burden. The residence time of BC was decreased from 8.4 to 4.3 days if insoluble BC was also scavenged by convection.

6. Sensitivity Studies

6.1. Experiments

[40] As shown in section 3 model simulated aerosol fields do not exactly match the available observations of

mass concentrations and AODs. This may arise from several factors including deficiency in the emissions, model transport, and treatment of aerosol aging and deposition. Some sensitivity tests can help to gain insights into these issues. We carry out sensitivity studies on the transformation time for conversion of hydrophobic to hydrophilic form and partitioning of the emissions between the hydrophobic and hydrophilic forms. We use the first year (1997) of our previous simulation as the control experiment (CONTROL). Further simulations have been performed for the same year and with the same spin-up but for different values of some of the parameters. The effects on the global distributions of BC and OM burdens, residence times, and AOD are compared to the CONTROL experiment and discussed in this section. The global aerosol budgets for these sensitivity experiments are summarized in Table 4.

6.2. Sensitivity to Emission Partitioning

[41] There is no clear information on how to partition carbonaceous aerosol emissions between the hydrophobic and hydrophilic forms. In most global models including

Table 3. Summary of the Global Budget of Carbonaceous Aerosols

Reference	Emissions, Tg BC/OC/OM yr ⁻¹	Dry Deposition, Tg BC/OC/OM yr ⁻¹	Wet Deposition, Tg BC/OC/OM	Burden, Tg BC/OC/OM	Residence Time ⁱ , days
BC					
<i>This study</i>	11.6	1.9 (16%)	9.7 (84%)	0.24	7.56
<i>Hydrophobic</i>	9.3	0.6 (5%) ^g	0.5 (4%) ^g	0.04	1.58
<i>Hydrophilic</i>	2.3 ^f	1.3 (11%) ^g	9.2 (80%) ^g	0.20	6.93
<i>Cooke and Wilson</i> [1996]	13.9			0.28	5.29
<i>Lioussse et al.</i> [1996]	12.3			0.13	4.00–4.50
<i>Cooke et al.</i> [1999] ^a	5.1			0.073	5.29
<i>Koch</i> [2001] ^b	12.41	4.5–5.2 (36–42%)	7.2–7.8 (58–64%)	0.14–0.29	4.28–8.42
<i>Chin et al.</i> [2002] ^c	17.5–18.7	3.8–4.2 (21–24%)	13.6–14.8 (76–79%)	0.28–0.32	5.70–6.30
<i>Chuang et al.</i> [2002]	12.2	2.7 (22%)	9.5 (78%)	0.20	5.97
<i>Chung and Seinfeld</i> [2002]	12.0	4.1 (34%)	7.9 (66%)	0.22	6.40
<i>Cooke et al.</i> [2002] ^a	5.1			0.06	4.29
OC					
<i>This study (OM)</i>	108.4	16.1 (15%)	92.4 (85%)	2.21	7.44
<i>Hydrophobic</i>	54.2	3.1 (3%) ^g	2.6 (2%) ^g	0.21	1.41
<i>Hydrophilic</i>	54.2 ^f	13.0 (12%) ^g	89.8 (83%) ^g	2.00	7.10
<i>Cooke et al.</i> [1999] ^a	7.0			0.087	4.54
<i>Koch</i> [2001] ^b	69.1	22.9 (33%)	46.2 (67%)	0.73	3.86
<i>Takemura et al.</i> [2000] ^d	105.8	19.2 (18%) ^h	86.6 (82%)	2.24	7.70
<i>Chin et al.</i> [2002] ^c	100.6–108.8	19.2–21.7 (18–21%)	80.6–88.7 (70–82%)	1.30–1.50	4.70–5.30
<i>Chuang et al.</i> [2002]	66.4	13.5 (20%)	52.9 (80%)	1.16	6.36
<i>Chung and Seinfeld</i> [2002] (OM) ^e	92.2	27.7 (30%)	64.5 (70%)	1.39	5.50
<i>Cooke et al.</i> [2002] ^a	14.0			0.13	3.39

^aOnly fossil fuels.

^bThe range of estimates arises from different scavenging schemes.

^cThe range of estimates is for different years.

^dSum of BC and OC.

^eSum of primary and secondary OM.

^fOnly direct emissions.

^gThe percentages of deposition for hydrophobic and hydrophilic fractions are relative to the total deposition.

^hAlso includes a sedimentation flux of 0.2 Tg yr⁻¹.

ⁱResidence time is estimated as the ratio of burden to the sources (or sinks) of a given species.

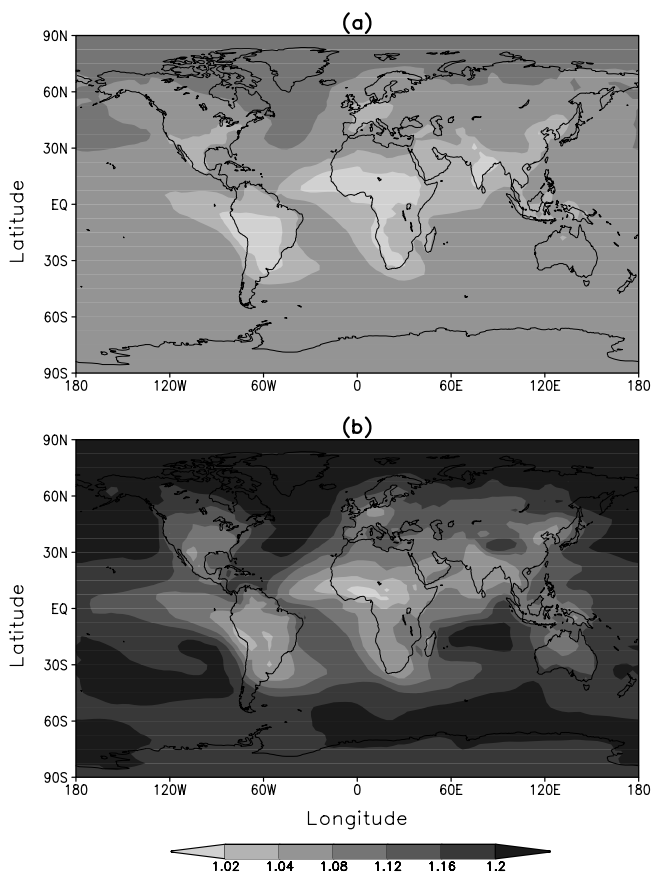


Figure 19. Ratio of (a) BC and (b) OM burdens from the HYDROPHOBIC experiment to that from the CONTROL experiment for the year 1997. See color version of this figure in the HTML.

this one BC is emitted as 80% hydrophobic and 20% hydrophilic while OM is emitted as 50% hydrophobic and 50% hydrophilic. Here we conduct a sensitivity test to this parameter by emitting 100% of BC and OM in hydrophobic form (experiment HYDROPHOBIC) or hydrophilic form (experiment HYDROPHILIC). In the model there is no in-cloud scavenging for hydrophobic aerosols so any increase in this fraction increases the aerosol burden and residence time.

[42] In HYDROPHOBIC the global BC burden and residence time increase by 4% and 0.25 days, respectively, as compared to the CONTROL experiment (Table 4). The increase is less over the source and outflow regions and larger over the remote regions (Figure 19a). The OM burden increases by 9% with a longer residence time of 0.64 days. The enhanced effect for OM as compared to BC (Figure 19b) is explained by the fact that in the CONTROL experiment 80% of BC, but only 50% of OM, are emitted as hydrophobic. We also observe an effect on the aerosol vertical distribution when the emission partitioning is changed (maps not shown). Over the 40°–90° NH and SH latitudinal bands, BC concentrations increase by 5–15% in the entire troposphere, with a maximum increase at 700–400 hPa. Patterns are similar but more pronounced for the concentrations of OM with

an increase up to 35% at about 500 hPa over the NH and SH midlatitudes. The changes in burdens translate into similar changes in the AOD, with a 5% increase in near source and outflow regions and a 15–20% increase in background regions (map not shown).

[43] In the HYDROPHILIC experiment the global BC burden decreases by 15% and we observe a 1.04 day shorter residence time as compared to the CONTROL experiment (Table 4). As expected this effect is smaller for OM with a decrease in burden and residence time of 9% and 0.61 days, respectively. Changes in the global distributions of BC and OM burdens in HYDROPHILIC are significant (Figure 20), up to 10% over the source regions and 20 to 30% in the remote regions. Once again we observe significant changes in the aerosol vertical distributions in the midlatitudes and polar regions, with a decrease in concentrations of up to 50 and 35% for BC and OM, respectively. The changes in the AOD distribution follow those in burdens convoluted with that of RH. With all carbonaceous aerosols emitted in hydrophilic form the AOD reduces by 5–10% over source regions and up to 25% over remote regions (map not shown).

[44] *Cooke et al.* [2002] examined the effect of emission partitioning on the distribution of fossil fuel BC. In the case of the HYDROPHOBIC experiment, our estimate of 4% increase in the global BC burden is smaller than their

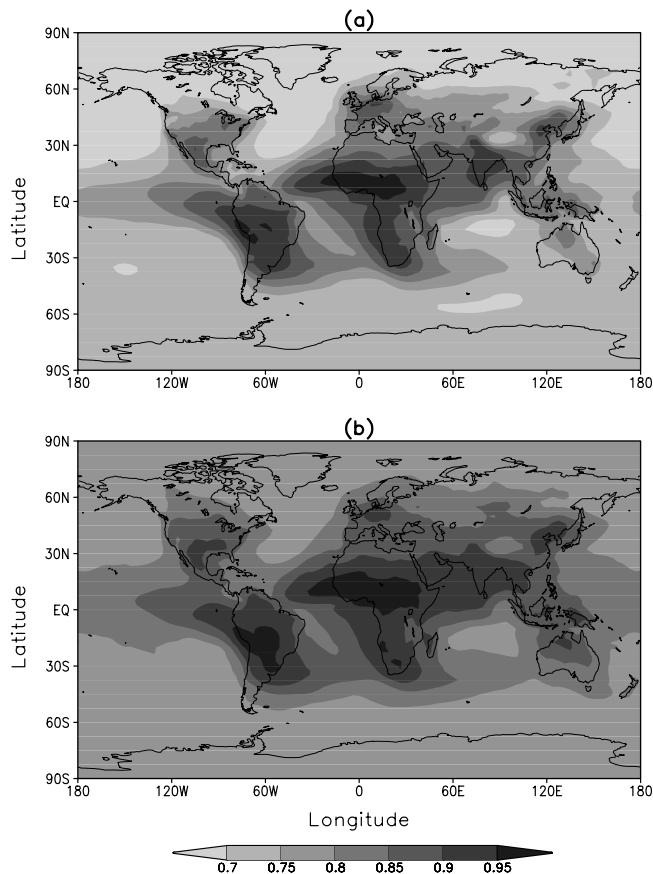


Figure 20. Same as Figure 19, but for the HYDROPHILIC experiment. See color version of this figure in the HTML.

Table 4. Global Budget for Carbonaceous Aerosols in the Sensitivity Experiments^a

Parameter	BC				OM			
	Dry Deposition	Wet Deposition	Burden	Residence Time	Dry Deposition	Wet Deposition	Burden	Residence Time
CONTROL	1.8	9.5	0.21	6.96	15.5	89.8	2.04	7.09
<i>Hydrophobic</i>	0.6	0.5	0.03	1.41	3.1	2.7	0.21	1.43
<i>Hydrophilic</i>	1.2	9.0	0.18	6.41	12.4	87.1	1.83	6.72
HYDROPHOBIC	1.9	9.4	0.22	7.21	15.9	89.4	2.22	7.73
<i>Hydrophobic</i>	0.7	0.6	0.04	1.42	6.0	5.3	0.41	1.43
<i>Hydrophilic</i>	1.2	8.9	0.18	6.55	9.9	84.1	1.81	7.05
HYDROPHILIC	1.7	9.6	0.18	5.92	14.8	90.5	1.85	6.48
<i>Hydrophobic</i>	0.0	0.0	0.00	—	0.00	0.0	0.00	—
<i>Hydrophilic</i>	1.7	9.6	0.18	5.92	14.8	90.5	1.85	6.48
λ halved	1.8	9.5	0.20	6.41	15.1	90.2	1.94	6.73
<i>Hydrophobic</i>	0.4	0.3	0.02	0.73	2.0	1.6	0.11	0.74
<i>Hydrophilic</i>	1.4	9.2	0.18	6.20	13.1	88.6	1.83	6.29
λ doubled	1.9	9.4	0.25	8.01	15.9	89.4	2.24	7.78
<i>Hydrophobic</i>	0.8	0.8	0.07	2.67	6.0	4.2	0.39	2.71
<i>Hydrophilic</i>	1.1	8.6	0.18	6.80	9.9	85.2	1.85	6.97

^aSimulations are for the year 1997 only. Same units as in Table 3.

estimate of 15%. In the case of the HYDROPHILIC experiment, our estimate of a 15% reduction in the BC burden is also smaller than their estimate of a 45% reduction. The difference is probably due to the fact that *Cooke et al.* [2002] only considered fossil fuel BC emissions which are concentrated over the relatively rainy regions of the globe (North America and Europe) as compared to biomass burning emissions which occur preferably during the dry season.

6.3. Sensitivity to Transformation Time

[45] Parameterizing the aging of carbonaceous aerosols through a conversion term from a hydrophobic to a hydrophilic form oversimplifies the actual physical and chemical processes at stake. Here we examine the sensitivity of the global aerosol burden to a doubling and halving of the transformation time used in the CONTROL experiment (1.63 days). The global BC burden decreases by 8% with halving and increases by 15% with doubling of the transformation time. At the same time the BC residence time decreases by 0.55 days with halving and increases by 1.05 days with doubling of the transformation time. The sensitivity of the OM burden and residence time to changes in the transformation time is similar to that of BC. Halving the transformation time results in a 5% reduction in OM burden and 0.26 days shorter residence time whereas doubling the transformation time results in a 10% increase in OM burden and 0.71 days longer residence time. Similarly to the emission partitioning experiments the largest relative changes in the aerosol vertical structure are found over polar regions at about 700–400 hPa. For instance an increase in BC concentrations of more than 60% is observed in these regions in the halving transformation time experiment.

[46] Our estimate of 8% reduction in BC burden for halving the transformation time is smaller than the estimate of 25% by *Cooke et al.* [2002], whereas our estimate of 15% increase in BC burden for doubling the transformation time is larger than *Cooke et al.* [2002] estimate of 7%. The reasons for the smaller sensitivity for the latter experiment of *Cooke et al.* [2002] are not clear. In addition to uncertainties in the emission partitioning and transformation time, uncertainties in the aerosol

emissions and deposition parameters also contribute to discrepancies between modeled and observed concentrations. Aerosol concentrations scale linearly with total emissions. Aerosol concentrations are more sensitive near the source regions as compared to remote regions to changes in the aerosol deposition parameterizations [*Cooke et al.*, 2002].

7. Contributions of Aerosols of Various Origins

[47] To assess the contribution of different source types (e.g., biomass, fossil fuels, and natural) to the global carbonaceous aerosol burden and AOD, we have carried out further simulations for 1997 with single source types. Biomass burning is the dominant source among three source types and accounts for 71% (0.15 Tg) and 78% (1.6 Tg) of BC and OM global annual average burdens, respectively (Table 5). Fossil fuel emissions contribute 29% (0.06 Tg) and 6% (0.12 Tg) to global BC and OM burdens, respectively. Natural sources (i.e., SOA) results only in OM and account for 16% (0.32 Tg) of the global OM burden. The SH is dominated by biomass burning emissions with contributions to BC and OM burdens of more than 80% over Africa, South America, and nearby oceanic regions (Figure 21, left panel). The contribution of fossil fuel emissions is significant only in the NH. Over Asia (India and China) the contribution of biomass burning sources to the BC burden is intermediate between those over the NH midlatitudes and the rest of the Tropics. The contributions of biomass burning and fossil fuel to the OM burden show similar patterns as for BC, but with lower values. The fossil fuel contribution to OM burden is largest over eastern Europe with values as large as 80% (Figure 21, middle panel). SOA from natural sources dominates over North America (contributions as large as 50%) with a 20 to 30% contribution over the oceans (Figure 21, right panel).

[48] There is a strong contrast between the tropics where biomass burning contributes more than 90% to the BC concentrations up to 400 hPa and the NH extratropics where the contribution is less than 20% up to 400 hPa (figure not shown). Features are same for OM concentrations but with a larger contribution of biomass

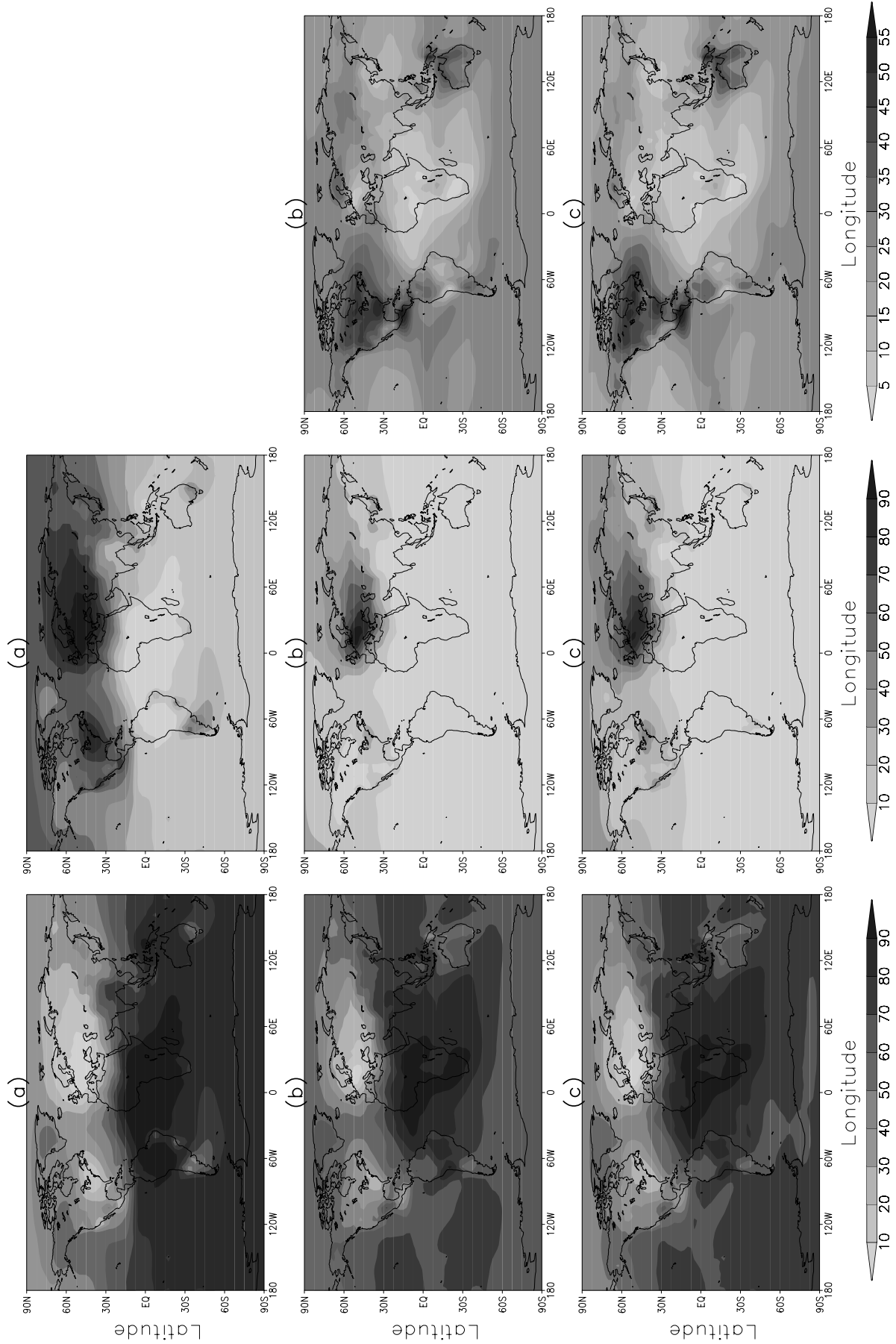


Figure 21

Table 5. Contribution of Different Source Types to Carbonaceous Aerosol Burdens and Optical Depth

Parameter/Source Type	SH Average	NH Average	Global Average
BC Burden, Tg BC	0.15	0.28	0.21
<i>Biomass</i>	0.13 (87%)	0.17 (61%)	0.15 (71%)
<i>Fossil fuels</i>	0.02 (13%)	0.11 (39%)	0.06 (29%)
<i>Natural</i>	—	—	—
OM burden, Tg OM	1.76	2.32	2.04
<i>Biomass</i>	1.43 (81%)	1.77 (76%)	1.60 (78%)
<i>Fossil fuels</i>	0.03 (2%)	0.22 (10%)	0.12 (6%)
<i>Natural</i>	0.30 (17%)	0.33 (14%)	0.32 (16%)
AOD (at 0.55 μm)	0.0241	0.0326	0.0283
<i>Biomass</i>	0.0197 (82%)	0.0232 (71%)	0.0214 (76%)
<i>Fossil fuels</i>	0.0007 (3%)	0.0043 (16%)	0.0029 (10%)
<i>Natural</i>	0.0037 (15%)	0.0051 (13%)	0.0040 (14%)

burning in the upper troposphere. OM from natural sources reaches pressure levels as high as 300 hPa at about 60°N and accounts for 40% of the total OM concentration.

[49] Consistently with the burdens, the AOD by carbonaceous aerosols is also dominated by biomass burning emissions with contributions of 76%, 71%, and 82% to the global, NH, and SH annual averages, respectively (Figure 21c and Table 5). The second largest contribution is from natural SOA (14%) and is roughly the same in both hemispheres. There is clear hemispheric contrast for the contribution of fossil fuel emissions to AOD, with a contribution in the NH (16%) which is a factor of 5 larger than in the SH (3%).

8. Conclusions

[50] In this study we have simulated the atmospheric cycle of carbonaceous aerosols in the LMDZT GCM and estimated the subsequent AOD. We include both BC and OM emissions from fossil fuel and biomass combustion, as well as some natural sources of secondary OM. The seasonal and interannual variability of open biomass burning emissions has been improved by combining existing emission inventories and satellite measured fire counts. The model performance has been thoroughly validated by comparing model results with available measurements in different parts of the globe. Over the United States, model estimates have been compared to regridded IMPROVE measurements, which eliminates the problem of comparing point measurements with a model grid-box value. The observed concentrations of BC are generally well reproduced by the model (i.e., within a factor of 2 for a majority of cases) but modeled OC concentrations are underestimated in comparison to many measurements. The discrepancy may be due to a mismatch between the emission base year (1984) and the time of measurements (most of them in the 1990s), lack of anthropogenic sources of secondary organic aerosols, or a real underestimation of the sources of primary organic aerosols.

[51] The burdens and residence times of BC and OM simulated in the LMDZT GCM are in the range of reported values in the literature. Both BC and OM have a residence time of slightly more than a week. The hydrophilic fraction of carbonaceous aerosols accounts for most of the atmospheric burden (90%). Aerosols emitted as hydrophobic are converted to hydrophilic form with a transformation time of 1.63 days, which results in a residence time of the hydrophobic fraction of 1.4–1.6 days. The distribution of AOD resembles that of the surface concentrations and burdens with peak values over the continents around the sources and outflow regions. On the global scale BC contributes 14% to the AOD by carbonaceous aerosols (0.031) with remaining 86% from OM and associated water.

[52] Some sensitivity tests have been carried out to understand the model response to changes in the transformation time and emission partitioning of carbonaceous aerosols. Aerosol burden, residence time, and optical depth change significantly among the different sensitivity studies. In all of the experiments the larger effects on aerosol burdens are found over the oceanic and polar regions. For our range of experiments where model parameters are varied within reasonable bounds the global BC and OM burden change within 15% and 10%, respectively. These changes occur through changes in the efficiency of aerosol wet deposition as aerosol is aging. The resulting changes in the BC and OM residence times are ± 1.0 and ± 0.7 days, respectively. A pronounced effect on the vertical aerosol structure is found in the free troposphere (700–400 hPa) over the midlatitudes and polar regions. It would be desirable to conduct sensitivity studies to emissions. However, the emission breakdown by sector and fuel type are usually not available.

[53] Biomass burning emissions are the dominant source of carbonaceous aerosols and account for 71% of BC and 78% of OM atmospheric burdens at the global scale. The optical depth by carbonaceous aerosols is also dominated by biomass burning sources over Africa and South America and more generally in the tropics. In contrast North America and Europe are dominated by emissions from fossil fuel and natural SOA and we observe a mix of both sources over Asia. On the global scale biomass burning emissions dominate the AOD (at 0.55 μm) with 76% of the total, followed by natural SOA with 14% and fossil fuel emissions with 10%.

[54] Long-term measurements of carbonaceous aerosols at different representative sites around the globe would provide a basis for a more complete model evaluation. In particular more measurements are required in the free and upper troposphere where we have found a large sensitivity of aerosol concentrations to our parameterizations. Estimation of the radiative effects of carbonaceous aerosols along with other aerosol species (sulfate, mineral dust, sea salt, and fly ash) is under way.

Figure 21. Fraction (%) of (a) BC burden, (b) OM burden, and (c) AOD which is due to biomass burning (left panels), fossil fuels (middle panels), and natural SOA emissions (right panels) for the year 1997. See color version of this figure in the HTML.

[55] **Acknowledgments.** We would like to thank anonymous reviewers for their thorough reading of the manuscript and constructive comments. This work was supported by the Environment and Climate Programme of the European Community (PHOENICS contract EVK2-CT-2001-00098). Computer time was provided by CNRS/IDRIS under projects 021167 and 031167. The Laboratoire d'Optique Atmosphérique is an institute of the "Fédération de Recherche" FR1818 of the CNRS. We thank AERONET PIs and their staff for establishing and maintaining the sites used in this study. We would like to acknowledge J. Ogren and the CMDL aerosol group for use of the absorption data from the CMDL sites.

References

- Adams, P. J., J. H. Seinfeld, D. M. Koch, L. Mickley, and D. Jacob (2001), General circulation model assessment of direct radiative forcing by sulfate-nitrate-ammonium-water inorganic aerosol system, *J. Geophys. Res.*, *106*, 1097–1112.
- Arino, O., M. Simon, I. Piccolini, and J. M. Rosaz (2001), The ERS-2 ATSR-2 world fire atlas and the ERS-2 ATSR-2 world burnt surface atlas projects, paper presented at 8th Conference on Physical Measurement and Signatures in Remote Sensing, Int. Soc. for Photogramm. and Remote Sensing, Aussois, France, 8–12 Jan.
- Balkanski, Y. J., D. J. Jacob, G. M. Gardner, W. C. Graustein, and K. K. Turekian (1993), Transport and residence times of tropospheric aerosols inferred from a global three-dimensional simulation of ^{210}Pb , *J. Geophys. Res.*, *98*, 20,573–20,586.
- Baltensperger, U., H. W. Gäggeler, D. T. Jost, M. Lugauer, M. Schwikowski, E. Weingartner, and P. Seibert (1997), Aerosol climatology at the high-Alpine site Jungfraujoch, Switzerland, *J. Geophys. Res.*, *102*, 19,707–19,715.
- Bhugwant, C., E. Rivière, P. Keckhut, and J. Leveau (2001), Variability of carbonaceous aerosols, ozone, and radon at Piton Textor, a mountain site on Réunion island (southwestern Indian Ocean), *Tellus, Ser. B*, *53*, 546–563.
- Bizjak, M., J. Turšič, M. Lešnjak, and T. Cegnar (1999), Air quality at Mt. Kravavec: Aerosol black carbon and ozone, *Acta Chim. Slov.*, *46*, 421–434.
- Bond, T. C., D. G. Streets, K. F. Yarber, S. M. Nelson, and I. J.-H. Woo (2004), A technology-based global inventory of black and organic carbon emissions from combustion, *J. Geophys. Res.*, *109*, doi:10.1029/2003JD003697, in press.
- Boucher, O., and T. L. Anderson (1995), GCM assessment of the sensitivity of direct climate forcing by anthropogenic sulfate aerosols to aerosol size and chemistry, *J. Geophys. Res.*, *100*, 26,117–26,134.
- Boucher, O., and U. Lohmann (1995), The sulfate-CCN-cloud albedo effect: A sensitivity study using two general circulation models, *Tellus, Ser. B*, *47*, 281–300.
- Boucher, O., and M. Pham (2002), History of sulfate aerosol radiative forcings, *Geophys. Res. Lett.*, *29*(9), 1308, doi:10.1029/2001GL014048.
- Boucher, O., M. Pham, and C. Venkataraman (2002), Simulation of the atmospheric sulfur cycle in the Laboratoire de Météorologie Dynamique general circulation model: Model description, model evaluation, and global and European budgets, *Note Sci. de l'IPSL*, *23*, 27 pp.
- Cachier, H. (1998), Carbonaceous combustion particles, in *Atmospheric Particles*, edited by R. M. Harisson and R. E. Van Grieken, pp. 295–348, John Wiley, Hoboken, N. J.
- Chin, M., P. Ginoux, S. Kinne, O. Torres, B. Holben, B. Duncan, R. Martin, J. Logan, A. Higurashi, and T. Nakajima (2002), Tropospheric aerosol optical thickness from the GOCART model and comparisons with satellite and sunphotometer measurements, *J. Atmos. Sci.*, *59*, 461–483.
- Chuang, C. C., J. E. Penner, J. M. Prospero, K. E. Grant, G. H. Rau, and K. Kawamoto (2002), Cloud susceptibility and the first aerosol indirect forcing: Sensitivity to black carbon and aerosol concentrations, *J. Geophys. Res.*, *107*(D21), 4564, doi:10.1029/2000JD000215.
- Chung, S. H., and J. H. Seinfeld (2002), Global distribution and radiative forcing of carbonaceous aerosols, *J. Geophys. Res.*, *107*(D19), 4407, doi:10.1029/2001JD001397.
- Cooke, W. F., and J. J. N. Wilson (1996), A global black carbon aerosol model, *J. Geophys. Res.*, *101*, 19,395–19,409.
- Cooke, W. F., C. Lioussé, H. Cachier, and J. Feichter (1999), Construction of a $1^\circ \times 1^\circ$ fossil fuel emission data set for carbonaceous aerosol and implementation and radiative impact in the ECHAM4 model, *J. Geophys. Res.*, *104*, 22,137–22,162.
- Cooke, W. F., V. Ramaswamy, and P. Kasibhatla (2002), A general circulation model study of the global carbonaceous aerosol distribution, *J. Geophys. Res.*, *107*(D16), 4279, doi:10.1029/2001JD001274.
- Crutzen, P. J., and M. G. Lawrence (2000), The impact of precipitation scavenging on the transport of trace gases: A 3-dimensional model sensitivity study, *J. Atmos. Chem.*, *37*, 81–112.
- Duncan, B. N., R. V. Martin, A. C. Staudt, R. Yevich, and J. A. Logan (2003), Interannual and seasonal variability of biomass burning emissions constrained by satellite observations, *J. Geophys. Res.*, *108*(D2), 4100, doi:10.1029/2002JD002378.
- Generoso, S., F.-M. Bréon, Y. Balkanski, O. Boucher, and M. Schulz (2003), Improving the seasonal cycle and interannual variations of biomass burning aerosol sources, *Atmos. Chem. Phys.*, *3*, 1211–1222.
- Gillani, N. V., S. E. Schwartz, W. R. Leaitch, J. W. Strapp, and G. A. Isaac (1995), Field observations in continental stratiform clouds: Partitioning of cloud particles between droplets and unactivated interstitial aerosols, *J. Geophys. Res.*, *100*, 18,687–18,706.
- Giorgi, F., and W. L. Chameides (1986), Rainout lifetimes of highly soluble aerosols and gases as inferred from simulations with a general circulation model, *J. Geophys. Res.*, *91*, 14,367–14,376.
- Guenther, A., et al. (1995), A global model of natural volatile organic compound emissions, *J. Geophys. Res.*, *100*, 8873–8892.
- Hauglustaine, D. A., F. Hourdin, L. Jourdain, M.-A. Filiberti, S. Walters, J.-F. Lamarque, and E. A. Holland (2004), Interactive chemistry in the Laboratoire de Météorologie Dynamique general circulation model: Description and background tropospheric chemistry evaluation, *J. Geophys. Res.*, *109*, D04314, doi:10.1029/2003JD003957.
- Haywood, J. M., and K. P. Shine (1995), The effect of anthropogenic sulfate and soot aerosol on the clear-sky planetary radiation budget, *Geophys. Res. Lett.*, *22*, 603–605.
- Höllner, R., S. Tohno, M. Kasahara, and R. Hitzenberger (2002), Long-term characterization of carbonaceous aerosol in Uji, Japan, *Atmos. Environ.*, *36*, 1267–1275.
- Horvath, H., J. Jäger, and C. Norek (1986), Determination of the size dependent light absorption coefficient of aerosols, *J. Aerosol Sci.*, *17*, 258–260.
- Hourdin, F., and A. Armangaud (1999), The use of finite-volume methods for atmospheric advection of trace species. Part I: Test of various formulations in a general circulation model, *Mon. Weather Rev.*, *127*, 822–837.
- Japar, S. M., W. W. Brachaczek, R. A. Gorse, J. M. Norbeck, and W. R. Pierson (1986), The contribution of elemental carbon to the optical properties of rural atmospheric aerosols, *Atmos. Environ.*, *20*, 1281–1289.
- Kanakidou, M. K., K. Tsigaridis, F. J. Dentener, and P. J. Crutzen (2000), Human activity enhanced formation of organic aerosols by biogenic hydrocarbon oxidation, *J. Geophys. Res.*, *105*, 9243–9254.
- Kaneyasu, N., S. Ohta, and N. Murao (1995), Seasonal variation in the chemical composition of atmospheric aerosols and gaseous species in Sapporo, Japan, *Atmos. Environ.*, *29*, 1559–1568.
- Kiehl, J. T., and B. P. Briegleb (1993), The relative roles of sulfate aerosols and greenhouse gases in climate forcing, *Science*, *260*, 311–314.
- Kim, Y. P., et al. (2000), Carbonaceous species in fine particles at the background sites in Korea between 1994 and 1999, *Atmos. Environ.*, *34*, 5053–5060.
- Koch, D. (2001), Transport and direct radiative forcing of carbonaceous and sulfate aerosols in the GISS GCM, *J. Geophys. Res.*, *106*, 20,311–20,332.
- Köpke, P., M. Hess, I. Schult, and E. P. Shettle (1997), Global aerosol data set, *Tech. Rep. 243*, pp. 103–158, Max Planck Inst., Hamburg, Germany.
- Lee, H. S., and B.-W. Kang (2001), Chemical characteristics of principal PM_{2.5} species in Chongju, South Korea, *Atmos. Environ.*, *35*, 739–746.
- Lioussé, C., H. Cachier, and S. G. Jennings (1993), Optical and thermal measurements of black carbon aerosol content in different environments: Variation of specific attenuation cross-section, sigma (σ), *Atmos. Environ.*, *27*, 1203–1211.
- Lioussé, C., J. E. Penner, C. Chuang, J. J. Walton, H. Eddleman, and H. Cachier (1996), A global three-dimensional model study of carbonaceous aerosols, *J. Geophys. Res.*, *101*, 19,411–19,432.
- Malm, W. C., M. L. Pitchford, M. Scraggs, J. F. Siskler, R. Ames, S. Copeland, K. A. Gebhart, and D. E. Day (2000), Spatial and seasonal patterns and temporal variability of haze and its constituents in the United States: Report III, Coop. Inst. for Res., Colo. State Univ., Fort Collins, Colo.
- Mari, C., D. J. Jacob, and P. Bechtold (2000), Transport and scavenging of soluble gases in a deep convective cloud, *J. Geophys. Res.*, *105*, 22,255–22,267.
- Nyeki, S., U. Baltensperger, I. Colbeck, D. T. Jost, E. Weingartner, and H. W. Gäggeler (1998), The Jungfraujoch high-Alpine research station (3454 m) as a background clean continental site for the measurement of aerosol parameters, *J. Geophys. Res.*, *103*, 6097–6107.
- Pandis, S. N., S. E. Paulson, J. H. Seinfeld, and R. C. Flagan (1991), Aerosol formation in the photooxidation of isoprene and beta-pinene, *Atmos. Environ., Part A*, *25*, 997–1008.

- Park, R. J., D. J. Jacob, M. Chin, and R. V. Martin (2003), Sources of carbonaceous aerosols over the United States and implications for natural visibility, *J. Geophys. Res.*, *108*(D12), 4355, doi:10.1029/2002JD003190.
- Park, S. S., Y. J. Kim, and K. Fung (2001), Characteristics of PM_{2.5} carbonaceous aerosol in the Sihwa industrial area, Korea, *Atmos. Environ.*, *35*, 657–665.
- Penner, J. E., H. Eddleman, and T. Novakov (1993), Toward the development of a global inventory for black carbon emissions, *Atmos. Environ., Part A*, *27*, 1277–1295.
- Penner, J. E., C. C. Chuang, and K. Grant (1998), Climate forcing by carbonaceous and sulfate aerosols, *Clim. Dyn.*, *14*, 839–851.
- Pruppacher, H. R., and J. D. Klett (1997), *Microphysics of Clouds and Precipitation, Second Revised and Enlarged Edition With an Introduction to Cloud Chemistry and Cloud Electricity*, 954 pp., Kluwer Acad., Norwell, Mass.
- Putaud, J.-P., et al. (2002), A European aerosol phenomenology: Physical and chemical characteristics of particulate matter at kerbside, urban, rural and background sites in Europe, 55 pp., Inst. for Environ. and Sustainability, Joint Res. Cent., Ispra, Italy. (Available at <http://ies.jrc.cec.eu.int/Download/cc/3>)
- Ramaswamy, V., O. Boucher, J. Haigh, D. Hauglustaine, J. Haywood, G. Myhre, T. Nakajima, G. Y. Shi, and S. Solomon (2001), Radiative forcing of climate change, in *Climate Change 2001, The Scientific Basis, Contribution of Working Group I to the Third Assessment Report of the IPCC*, edited by J. T. Houghton et al., chap. 6, pp. 349–416, Cambridge Univ. Press, New York.
- Reddy, M. S., and C. Venkataraman (2002a), Inventory of aerosol and sulphur dioxide emissions from India: I – Fossil fuels combustion, *Atmos. Environ.*, *36*, 677–697.
- Reddy, M. S., and C. Venkataraman (2002b), Inventory of aerosol and sulphur dioxide emissions from India: II – Biomass combustion, *Atmos. Environ.*, *36*, 699–712.
- Schultz, M. G. (2002), On the use of ATSR fire count data to estimate the seasonal and interannual variability of vegetation fire emissions, *Atmos. Chem. Phys.*, *2*, 387–395.
- Streets, D. G., et al. (2003), An inventory of gaseous and primary aerosol emissions in Asia in the year 2000, *J. Geophys. Res.*, *108*(D21), 8809, doi:10.1029/2002JD003093.
- Takemura, T., H. Okamoto, Y. Maruyama, A. Numaguti, A. Higurashi, and T. Nakajima (2000), Global three-dimensional simulation of aerosol optical thickness distribution of various origins, *J. Geophys. Res.*, *105*, 17,853–17,873.
- Tang, I. N., and H. R. Munkelwitz (1994), Water activities, densities, and refractive indices of aqueous sulfates and sodium nitrate droplets of atmospheric importance, *J. Geophys. Res.*, *99*, 18,801–18,808.
- Tiedtke, M. (1989), A comprehensive mass flux scheme for cumulus parameterization in large-scale models, *Q. J. R. Meteorol. Soc.*, *117*, 1779–1800.
- Tsigaridis, K., and M. Kanakidou (2003), Global modeling of secondary organic aerosol in the troposphere: A sensitivity analysis, *Atmos. Chem. Phys. Discuss.*, *3*, 2879–2929.
- Turpin, B. J., and H.-J. Lim (2002), Species contributions to PM_{2.5} mass concentrations: Revisiting common assumptions for estimating organic mass, *Aerosol Sci. Technol.*, *35*, 602–610.
- van Leer, B. (1977), Toward the ultimate conservative difference scheme: IV. A new approach to numerical convection, *J. Comput. Phys.*, *23*, 276–299.
- Viidanoja, J., M. Sillanpää, J. Laakia, V.-M. Kerminen, R. Hillamo, P. Aarnio, and T. Koskentalo (2002), Organic and black carbon in PM_{2.5} and PM₁₀: 1 year of data from an urban site in Helsinki, Finland, *Atmos. Environ.*, *36*, 3183–3193.
- Wolff, E. W., and H. Cachier (1998), Concentrations and seasonal cycle of black carbon in aerosol at a coastal Antarctic station, *J. Geophys. Res.*, *103*, 11,033–11,041.

O. Boucher and M. S. Reddy, Laboratoire d'Optique Atmosphérique, UFR de Physique, CNRS UMR 8518/Université des Sciences et Technologies de Lille, 59655 Villeneuve d'Ascq Cedex, France. (boucher@loa.univ-lille1.fr; reddy@loa.univ-lille1.fr)